Microcircuits of excitatory and inhibitory neurons in layer 2/3 of mouse barrel cortex

Michael Avermann, Christian Tomm, Celine Mateo, Wulfram Gerstner and Carl C. H. Petersen

J Neurophysiol 107:3116-3134, 2012. First published 7 March 2012;
doi: 10.1152/jn.00917.2011

J Neurophysiol 107: 3116–3134, 2012.
First published March 7, 2012; doi:10.1152/jn.00917.2011.

Microcircuits of excitatory and inhibitory neurons in layer 2/3 of mouse barrel cortex

Michael Avermann,[1] Christian Tomm,[2] Celine Mateo,[1,3] Wulfram Gerstner,[2] and Carl C. H. Petersen[1]
[1]*Laboratory of Sensory Processing, Brain Mind Institute, Faculty of Life Sciences, École Polytechnique Fédérale de Lausanne (EPFL), Lausanne, Switzerland;* [2]*School of Computer and Communication Sciences and School of Life Sciences, Brain Mind Institute, EPFL, Lausanne, Switzerland; and* [3]*Department of Physics, University of California, San Diego, California*

Submitted 7 October 2011; accepted in final form 1 March 2012

Avermann M, Tomm C, Mateo C, Gerstner W, Petersen CC. Microcircuits of excitatory and inhibitory neurons in layer 2/3 of mouse barrel cortex. *J Neurophysiol* 107: 3116–3134, 2012. First published March 7, 2012; doi:10.1152/jn.00917.2011.—Synaptic interactions between nearby excitatory and inhibitory neurons in the neocortex are thought to play fundamental roles in sensory processing. Here, we have combined optogenetic stimulation, whole cell recordings, and computational modeling to define key functional microcircuits within layer 2/3 of mouse primary somatosensory barrel cortex. In vitro optogenetic stimulation of excitatory layer 2/3 neurons expressing channelrhodopsin-2 evoked a rapid sequence of excitation followed by inhibition. Fast-spiking (FS) GABAergic neurons received large-amplitude, fast-rising depolarizing postsynaptic potentials, often driving action potentials. In contrast, the same optogenetic stimulus evoked small-amplitude, subthreshold postsynaptic potentials in excitatory and non-fast-spiking (NFS) GABAergic neurons. To understand the synaptic mechanisms underlying this network activity, we investigated unitary synaptic connectivity through multiple simultaneous whole cell recordings. FS GABAergic neurons received unitary excitatory postsynaptic potentials with higher probability, larger amplitudes, and faster kinetics compared with NFS GABAergic neurons and other excitatory neurons. Both FS and NFS GABAergic neurons evoked robust inhibition on postsynaptic layer 2/3 neurons. A simple computational model based on the experimentally determined electrophysiological properties of the different classes of layer 2/3 neurons and their unitary synaptic connectivity accounted for key aspects of the network activity evoked by optogenetic stimulation, including the strong recruitment of FS GABAergic neurons acting to suppress firing of excitatory neurons. We conclude that FS GABAergic neurons play an important role in neocortical microcircuit function through their strong local synaptic connectivity, which might contribute to driving sparse coding in excitatory layer 2/3 neurons of mouse barrel cortex in vivo.

excitatory neurons; inhibitory neurons; neocortex; synaptic transmission

EXCITATORY AND INHIBITORY NEURONS interact strongly through synaptic connections within neocortical microcircuits to process sensory information. To mechanistically understand the functional operation of neocortical neuronal networks, it will be essential to quantitatively map the synaptic connectivity between different classes of neurons. On the basis of such data, it may then be possible to computationally model simplified neuronal networks, which might reveal insights into the basic functional architecture of neocortical circuits.

Address for reprint requests and other correspondence: C. C. H. Petersen, Laboratory of Sensory Processing, Brain Mind Institute, Faculty of Life Sciences, SV-BMI-LSENS, Station 19, École Polytechnique Fédérale de Lausanne (EPFL), CH-1015 Lausanne, Switzerland (e-mail: carl.petersen@epfl.ch).

Synaptic connectivity of nearby neurons can be analyzed in brain slices in vitro through simultaneous recordings of presynaptic and postsynaptic neurons. Previous studies have found that nearby excitatory neocortical pyramidal neurons are synaptically connected with ~15% probability and that the majority of unitary excitatory postsynaptic potentials (uEPSPs) are small in amplitude with only a few large-amplitude connections (Brown and Hestrin 2009; Feldmeyer et al. 2006; Holmgren et al. 2003; Ko et al. 2011; Lefort et al. 2009; Markram et al. 1997; Perin et al. 2011; Song et al. 2005; Thomson and Lamy 2007). In contrast, synaptic connectivity between excitatory pyramidal neurons and some types of inhibitory GABAergic neurons of the neocortex has been reported to be much stronger (Bock et al. 2011; Chittajallu and Isaac 2010; Fino and Yuste 2011; Helmstaedter et al. 2008; Hofer et al. 2011; Holmgren et al. 2003; Kapfer et al. 2007; Molnár et al. 2008; Oláh et al. 2009; Packer and Yuste 2011; Reyes et al. 1998; Silberberg and Markram 2007; Sun et al. 2006).

In this study, we quantitatively analyzed synaptic connectivity in layer 2/3 of mouse primary somatosensory barrel cortex (Lübke and Feldmeyer 2007; Petersen 2007; Schubert et al. 2007), differentiating between excitatory pyramidal neurons and inhibitory GABAergic neurons through green fluorescent protein (GFP) expression in GAD67-GFP knockin mice, in which nearly all layer 2/3 GABAergic neurons express GFP (Gentet et al. 2010; Tamamaki et al. 2003). We first investigated network activity driven by optogenetic stimulation of layer 2/3 excitatory neurons, and we then examined unitary connectivity through multiple simultaneous whole cell recordings. Finally, we used simple computational neuronal network models to test our understanding of synaptic interactions within the layer 2/3 microcircuit. We found that fast-spiking parvalbumin-expressing GABAergic neurons are highly synaptically connected to nearby neurons and thereby play a central role in governing neocortical network behavior. Such analysis of synaptic connectivity helps toward a mechanistic understanding of the in vivo neuronal network activity recorded in layer 2/3 barrel cortex of GAD67-GFP mice, where we found high firing rates of GABAergic neurons but sparse action potential (AP) firing in excitatory neurons (Crochet et al. 2011; Gentet et al. 2010; Mateo et al. 2011).

MATERIALS AND METHODS

All animal experiments were carried out under protocols approved by the Swiss Federal Veterinary Office.

Lentivirus production and stereotactic virus injections. Virus production was based on transient transfection of human embryonic

kidney 293T cells with self-inactivating lentiviral vector constructs (Deglon et al. 2000). The following plasmids were used for virus production: pCMVΔ8.92 (packaging plasmid), pRSV-Rev (encoding the Rev protein of human immunodeficiency virus type 1), pMD2G (vesicular stomatitis virus G protein envelope), and the hChR2-mCherry transfer vector (humanized channelrhodopsin-2-mCherry fusion protein; kind gift of Karl Deisseroth, Stanford University, Stanford, CA). Viral supernatants were harvested 48 h after transfection. The supernatants were filtered through 22-μm vacuum filters and concentrated ~1,000 times by ultracentrifugation in a SW28 rotor (Beckman Coulter). The efficiency of vector production and packaging was monitored by determining the total vector concentration with an anti-P24 ELISA immunoassay (Gentaur). The P24 concentration of the vector was ~150,000 ng/ml. Virus was stored in PBS at −80°C.

Lentivirus was stereotactically injected into the barrel cortex of GAD67-GFP knockin mice (Tamamaki et al. 2003) of either sex at postnatal *day 9*. Injections were carried out under deep isoflurane anesthesia (2%), and paw-withdrawal reflex was absent. The animals were maintained on a heating blanket at 37°C. Approximately 80 nl of virus solution were injected directly into the barrel cortex at a target depth of 300 μm below the pia. Before the injection pipette was retracted, the virus was given an additional ~5 min to diffuse. The pups then recovered from anesthesia under a heat lamp for ~30 min before being returned to their mother.

Slice preparation. The brains of GAD67-GFP mice of either sex were removed at postnatal *days 17–22* (8–13 days after viral injections for the ChR2 experiments), and 300-μm- thick parasagittal (35° away from vertical) brain slices were cut on a vibrating slicer (Leica VT1000S) in an ice-cold modified artificial cerebrospinal fluid (ACSF) (Bureau et al. 2006; Lefort et al. 2009) containing (in mM) 110 choline chloride, 25 $NaHCO_3$, 25 D-glucose, 11.6 sodium ascorbate, 7 $MgCl_2$, 3.1 sodium pyruvate, 2.5 KCl, 1.25 NaH_2PO_4, and 0.5 $CaCl_2$. After being sliced, the tissue was transferred to a chamber with standard ACSF, containing (in mM) 125 NaCl, 25 $NaHCO_3$, 25 D-glucose, 2.5 KCl, 1.25 NaH_2PO_4, 2 $CaCl_2$, and 1 $MgCl_2$, aerated with 95% O_2-5% CO_2 at 33°C for 15 min. Subsequently, slices were maintained at room temperature until the recording session started (within 4 h of slicing).

Two-photon microscopy and electrophysiological recordings. For ChR2 experiments, the brain slices containing ChR2-mCherry-expressing cells were identified with a ×4 objective lens (Olympus UPlanFI 4×, 0.13 NA) using brief illumination with 580-nm light (Chroma Technology HQ580/20) to excite mCherry fluorescence, without activating ChR2-expressing neurons. GFP-expressing GABAergic neurons were visualized using a two-photon microscope (Prairie Technologies). Infrared excitation light of 880 nm was generated by a MaiTai laser (SpectraPhysics) and focused into the slice tissue with a ×40, 0.8-NA water-immersion objective (Olympus). Creation of a gradient contrast image of unlabeled cells, precisely aligned to the GFP fluorescence image, was achieved by detecting the scanned transmitted infrared light through a Dodt contrast element (Luigs and Neumann). Brain slices were continually superfused with ACSF at 32°C and aerated with 95% O_2-5% CO_2.

Neurons were recorded in whole cell configuration with Multiclamp 700B amplifiers (Molecular Devices). Borosilicate patch pipettes with resistance of 5–7 MΩ were used. The pipette intracellular solution contained (in mM) 135 K-gluconate, 4 KCl, 4 Mg-ATP, 10 Na_2-phosphocreatine, 0.3 Na-GTP, and 10 HEPES (pH 7.3, 280 mosmol/l). Biocytin (3 mg/ml) and Alexa-594 hydrazide (10 μM) were added to the intracellular solution. Electrophysiological data were low-pass Bessel filtered at 10 kHz and digitized at 20 kHz with an ITC-18 acquisition board (Instrutech). Data acquisition routines were custom-made procedures written in IgorPro software (Wavemetrics). Membrane potential measurements were not corrected for the liquid junction potential. Image stacks of cells filled with Alexa-594 dye were taken at the end of each recording session and consisted of optical sections separated by 2.5 μm, taken at an image resolution of 512 × 512 pixels and a dwell time of 8 μs/pixel.

Extracellular recordings of light-evoked APs in ChR2-expressing neurons were performed in loose-patch mode with 25 μM 6-cyano-7-nitroquinoxaline-2,3-dione (CNQX) and 25 μM D-2-amino-5-phosphonovaleric acid (APV) added to the extracellular medium. The same type of pipettes as used for whole cell recordings were filled with HEPES-buffered Ringer solution (pH 7.3), and a seal of 8–10 MΩ between a neuron and the pipette was formed by gentle suction to obtain a good signal-to-noise ratio.

For stimulation of ChR2-expressing neurons, we used a 470-nm collimated blue LED system (Thorlabs) coupled to the epifluorescence light path of an BX51WI microscope (Olympus) and focused onto the brain slice via a ×40, 0.8-NA water-immersion objective (Olympus). Whole field blue light stimulation intensity was ~5.6 mW/mm^2 with a duration of 3 ms.

Analysis of electrophysiological data. Electrophysiological data were analyzed using custom-made routines written in IgorPro software (Wavemetrics). Mean traces were calculated by averaging over 25 single trials. Intrinsic electrophysiological properties of neurons were tested directly after break-in by injection of 500-ms square current pulses incrementing in 20-pA steps, starting at −100 pA. Resting membrane potential (V_m) was calculated from a 5-ms average before current injection. The average membrane time constant (τ) was extracted from an exponential fit from the time of current stimulus onset until the time of stimulus offset. The total series resistance was calculated from the current-voltage (*I-V*) relationship of the obtained traces. Each voltage deflection was calculated from a 50-ms average at the end of the current injection trace. The slope of a linear fit to the *I-V* curve was determined as the total series resistance. The input resistance of the cell (R_{in}) was obtained by subtracting the access resistance. AP threshold was calculated by determining the time point of the first peak of the third derivative of the average AP. AP threshold was defined as the corresponding time point on the voltage trace. AP threshold was corrected for access resistance. AP amplitude was calculated from AP threshold to the peak of the AP. The AP half-width was defined as the width of the AP at half-maximal amplitude. To obtain the neuron's maximum firing frequency, depolarizing currents in 20-pA steps were injected until the number of APs per stimulus reached a plateau phase. Rheobase was defined as the minimum current required to evoke an AP during the 500 ms of sustained somatic current injections. Postsynaptic potential (PSP) baselines were defined as the mean V_m 5 ms before stimulus onset. PSP amplitudes were defined as the difference between baseline and the mean voltage averaged across 0.5 ms at ±0.25 ms around the peak of the averaged PSP. The PSP half-width was calculated as the width of the PSP at half-maximal amplitude. The PSP rise time was computed as the time difference from 20% to 80% of the PSP amplitude. The slope of the PSP was calculated from a linear fit to the 20–80% rise-time period. The PSP onset latency was computed by detecting the time point after the peak of the presynaptic AP at which the voltage trace deflects from the average V_m and does not cross it until the end of the PSP. Onset latency was defined as the time difference between this point and the time of the presynaptic AP peak.

Assessment of statistical differences was carried out in Prism5 software (GraphPad). For the analysis of intrinsic electrophysiological parameters and PSP parameters, if more than two unpaired groups of data were analyzed, then the nonparametric Kruskal-Wallis test followed by Dunn's posttest for multiple comparisons was chosen to compute statistics for independent samples (see Fig. 1, *B–G*; Fig. 5, *B, C, E–G, I*; Fig. 6, *D–F*; and Table 2). Statistical differences between paired data groups were analyzed using a paired *t*-test (Fig. 4*D*). Correlations between two parameters were assessed by computing the nonparametric Spearman correlation coefficient (Fig. 3*E*). Differences in AP probability and connectivity between different classes of neurons were assessed by using a χ^2 test on contingency tables (see Fig. 5*D*, Fig. 6*C*, Fig. 7*B*, and Table 2). Comparisons of the proba-

bilities of reciprocal bidirectional synaptic connections were analyzed with a binomial test (see Table 4). All experimental data are means ± SE, except where specifically indicated otherwise.

Immunohistochemistry. All steps were carried out on a horizontal shaker, and each step was followed by extensive washing in PBS (pH 7.4). After recording was carried out, brain slices were fixed in 4% PFA for 2 h at room temperature. For diaminobenzidine (DAB) staining after the immunohistochemistry, slices were incubated in 1% H_2O_2 to quench endogenous peroxidases. Slices were then incubated overnight in 30% sucrose solution for subsequent permeabilization steps by four repeated freeze-thaw cycles over liquid nitrogen. Slices were blocked in a solution containing 5% normal goat serum (Uptima) in PBS for 1 h at room temperature and then incubated in the primary anti-parvalbumin (PV) antibody (1:2,000; PV28; Swant) for a minimum of 3 days at 4°C. After incubation in the primary antibody, slices were treated with Alexa-594-conjugated goat anti-rabbit IgG (1:200; Vector Laboratories) and Alexa-405-conjugated streptavidin (1:200; Invitrogen) for 2 h at room temperature. DAPI (4′,6-diamidino-2-phenylindole) was applied for 15 min at room temperature.

To perform DAB staining after confocal imaging, slices were mounted on a microscope slide in PBS without sealing. Images of the stained cells were acquired using a confocal Leica SP2 inverted microscope. Image stacks with optical sections separated by 2.5 μm were taken with a ×40, 1.25-NA oil lens at an image resolution of 1,024 × 1,024 pixels. For PV colocalization experiments, slices were additionally imaged in XZY mode to verify that antibody penetration was deep enough to reach the biocytin-filled somata of recorded neurons. Antibody penetration was usually in a range of 50–100 μm. If no DAB staining was to be performed afterwards, slices were mounted in DABCO (1,4-diazabicyclooctane).

After staining with PV antibodies was carried out, biocytin-filled cells were developed by performing DAB staining. Slices were conjugated with avidin-biotinylated peroxidase (ABC standard kit; Vector Laboratories) for 2 h at room temperature. Biocytin was revealed using a DAB-Ni complex and 0.002% H_2O_2. The enzymatic reaction was monitored under visual control and stopped by washing in PBS when the neuronal anatomy was clearly visible. To prevent squashing of mounted brain slices during the morphological reconstruction process, a 300-μm-thick frame (Abgene) was glued between coverslip and microscope slide. To prevent mounted slices from drying out, the edges of the coverslips were sealed with epoxy glue (Loctite 3430). Mounted slices were stored in the dark at 4°C. Three-dimensional morphological reconstructions were performed under a BX51WI bright-field microscope equipped with a ×100, 1.4-NA oil objective using Neurolucida (MicroBrightField).

Network simulations. The simulation of the layer 2/3 network was done using the NEST simulator (Gewaltig and Diesmann 2007) interfaced via pyNN (Davison et al. 2008). Three neuronal populations were chosen for the model: 1,961 excitatory neurons; 97 fast-spiking (FS) inhibitory GABAergic neurons, and 133 non-fast-spiking (NFS) inhibitory GABAergic neurons. The number of neurons in each cell class was chosen by following experimentally determined values for the C2 column of layer 2/3 mouse barrel cortex (Gentet et al. 2010; Lefort et al. 2009). Single neurons in each of these populations were simulated using the AdEx neuron model (Brette and Gerstner 2005). Intrinsic membrane parameters for individual neurons in the model (V_m, AP threshold, τ, and R_{in}) were directly taken from the distribution of experimental measurements on a single-cell basis (see mean data in Table 1). Synaptic conductance time constants were chosen to fit the mean experimental unitary PSP kinetics (see Table 3). For all other model parameters, standard values were used (Brette and Gerstner 2005). Synaptic connections in the network were constructed in a random fashion, based on the measured probabilities of synaptic connections between the specific types of neurons (see Table 2). The synaptic strengths of these connections were drawn from a lognormal fit of the measured distribution of PSP amplitudes (see mean, median, and range in Table 2).

To simulate the optogenetic stimulation paradigm, we excited a random set of excitatory neurons with a short current pulse to drive a spike. The number of neurons stimulated was systematically varied and the evoked response of the postsynaptic neurons in the network analyzed. We measured the peak amplitude of the depolarization in the postsynaptic membrane potential following the stimulus, as well as the number of evoked postsynaptic spikes. Similar analyses were also carried out in reduced versions of the model network in which inhibition mediated by either FS GABAergic neurons or NFS GABAergic neurons was specifically removed. To simulate an UP state, we used in vivo measurements of membrane potentials and AP thresholds of excitatory, FS GABAergic, and NFS GABAergic neurons (Mateo et al. 2011). Single neurons were depolarized to the UP state membrane potentials by injection of a step current. For the simulated UP state, we measured the number of postsynaptic neurons that emitted a spike in response to the stimulus. All computational modeling data are means ± SD.

RESULTS

Intrinsic electrophysiological properties of neurons in layer 2/3 mouse barrel cortex. In vitro whole cell recordings of membrane potential were obtained from layer 2/3 neurons located in primary somatosensory barrel cortex of GAD67-GFP mice, in which nearly all layer 2/3 GABAergic neurons express GFP (Tamamaki et al. 2003; Gentet et al. 2010). The whole cell recording electrodes contained the red fluorescent dye Alexa-594, allowing high-resolution two-photon imaging of the structure of the recorded neurons (Fig. 1*A*). Colocalization of green (GFP) and red (Alexa-594) fluorescence indicated that the recording was from an inhibitory GABAergic neuron, whereas the absence of GFP classified the recording of an excitatory glutamatergic neuron. GABAergic neurons were further subdivided into two categories depending on AP waveform. GFP-labeled GABAergic neurons were defined to be fast spiking (FS) if the AP had a duration at half-maximal amplitude of <0.75 ms (measured from threshold), whereas they were classified as non-fast spiking (NFS) if the AP waveform was of a longer duration (Fig. 1, *A* and *B*, Fig. 2, Table 1). Excitatory neurons had significantly broader APs than both classes of GABAergic neurons (Fig. 1*B* and Table 1). Several further electrophysiological features differentiated these three classes of layer 2/3 neurons. The resting V_m of NFS GABAergic neurons was significantly depolarized relative to FS GABAergic and excitatory neurons (Fig. 1*C* and Table 1). However, AP threshold was not different between any of the cell types (Table 1). The somatic R_{in} was significantly different between all three classes, with the highest R_{in} value in NFS GABAergic neurons and the lowest in FS GABAergic neurons (Fig. 1*D* and Table 1). Presumably as a result of these differences in V_m and R_{in}, NFS GABAergic neurons were found to be significantly more excitable than excitatory neurons, which in turn were more excitable than FS GABAergic neurons (excitability was measured as the minimal current needed to evoke an AP during a 500-ms depolarization, termed rheobase) (Fig. 1*E* and Table 1). The membrane time constant in response to hyperpolarizing current injection was fastest for FS GABAergic neurons, with excitatory neurons showing the slowest membrane time constants (Fig. 1*F* and Table 1). The maximal steady-state firing frequency was estimated as the asymptotic AP rate in response to increasing amplitudes of depolarizing current. Maximal firing rates were significantly different between all three classes of neurons, with FS GABAergic neurons firing at much

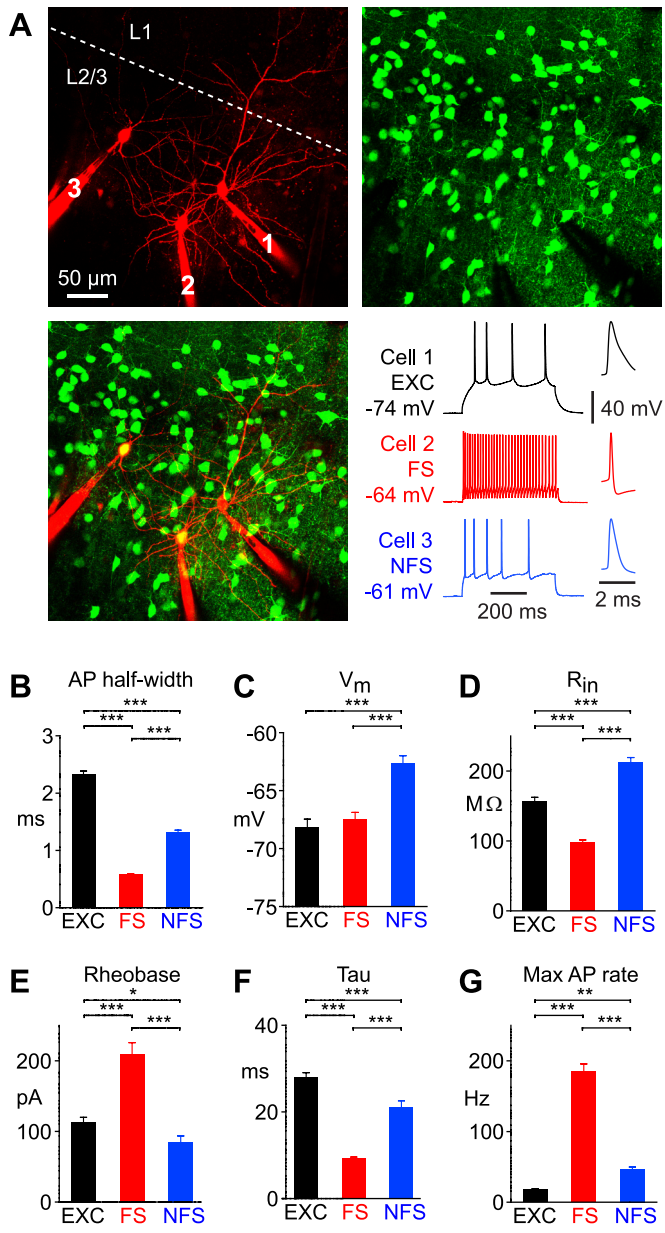

Fig. 1. Intrinsic electrophysiological properties of excitatory and inhibitory neurons in layer 2/3 (L2/3) mouse barrel cortex. *A*: example in vitro whole cell recordings targeted to excitatory and inhibitory neurons in GAD67-GFP knockin mice. Images are maximum intensity projections of a 2-photon *z* stack. Red fluorescence corresponds to Alexa-594 in the recording pipettes, which subsequently diffuses into the recorded neurons (*top left*, with border between L1 and L2/3 indicated by dashed line). Green fluorescence corresponds to green fluorescent protein (GFP)-labeling of GABAergic neurons (*top right*), which is shown in yellow in the overlay with red fluorescence (*bottom left*). The action potential (AP) firing patterns evoked by sustained somatic current injections of 500-ms duration from these neurons (*bottom right*; *insets* show a temporal zoom of the AP waveforms). *B*: AP half-width in excitatory (EXC), fast-spiking (FS) GABAergic, and non-fast-spiking (NFS) GABAergic neurons. *C*: resting membrane potential (V_m) across cell types. *D*: input resistance (R_{in}) across cell types. *E*: rheobase (minimal amplitude of 500-ms current pulse needed to evoke an AP) across cell types. *F*: membrane time constant (τ) across cell types (exponential fit to membrane potential change evoked by hyperpolarizing current step). *G*: maximum firing frequency across cell types. Data are means ± SE. $^*P < 0.05$; $^{**}P < 0.01$; $^{***}P < 0.001$, statistical significance according to nonparametric Kruskal-Wallis test followed by Dunn's posttest. See also Table 1.

higher maximal frequencies compared with NFS GABAergic neurons, which in turn were able to fire at higher frequencies than excitatory neurons (Fig. 1*G*, Fig. 2*E*, and Table 1).

Anatomical features and PV expression. During the whole cell recording, neurons were filled with biocytin for post hoc anatomical analysis. Excitatory neurons were pyramidal (layer 3) or modified pyramidal (layer 2) neurons with complex dendritic arborizations and relatively simple axons descending toward deeper layers with local collaterals mainly in layers 2, 3, and 5 (Fig. 2*A*) (Feldmeyer et al. 2006; Lübke et al. 2003). FS and NFS GABAergic neurons had relatively simple dendritic arborizations compared with excitatory neurons (Fig. 2, *A–C*), with overall shorter total dendritic length (excitatory: 5,387 ± 166 μm, $n = 4$; FS: 3,023 ± 320 μm, $n = 4$; NFS: 2,644 ± 209 μm, $n = 3$) and fewer branch-point nodes (excitatory: 54 ± 2 nodes, $n = 4$; FS: 23 ± 1 nodes, $n = 4$; NFS; 25 ± 3 nodes, $n = 3$). FS GABAergic neurons had more complex and denser local axonal arborizations compared with excitatory neurons and NFS GABAergic neurons (Fig. 2, *A–C*), with a longer local axonal length (excitatory: 3,665 ± 228 μm, $n = 3$; FS: 6,467 ± 759 μm, $n = 4$; NFS: 3,038 ± 876 μm, $n = 3$) containing more branch-point nodes (excitatory: 29 ± 3 nodes, $n = 3$; FS: 80 ± 12 nodes, $n = 4$; NFS: 39 ± 4 nodes, $n = 3$). These anatomical analyses are likely to underestimate the full extent of the neuronal structures because of truncation of neurites during the slicing procedure for preparation of in vitro brain slices, potentially incomplete biocytin filling of thin neuronal structures (especially axons), and the difficulties in tracing thin neuronal structures (especially axons) visualized with a light microscope.

Substantial evidence supports the expression of the calcium-binding protein PV in fast-spiking inhibitory neocortical neurons with narrow AP waveforms (Cauli et al. 1997; Kawaguchi and Kubota 1993; Kawaguchi 1995), but there are also reports of PV expression in some classes of inhibitory neurons with broader AP waveforms (Blatow et al. 2003; Runyan et al. 2010). We therefore specifically examined PV expression under our experimental conditions in GABAergic neurons of layer 2/3 mouse barrel cortex (Fig. 2, *B–D*). We found a clear and unambiguous correlation between AP waveform and PV expression. Every tested FS GABAergic neuron expressed PV (14 of 14 neurons), and every tested NFS GABAergic neuron did not express PV (29 of 29 neurons). These NFS GABAergic neurons may overlap substantially with a recently identified large class of 5-HT_{3A}-receptor-expressing and PV-negative GABAergic neurons in mouse somatosensory cortex (Lee et al. 2010). The broadest AP half-width in our population of PV-expressing GABAergic neurons was 0.65 ms, and the mean ± SE was 0.50 ± 0.02 ms ($n = 14$) (Fig. 2*D*). In contrast, the narrowest AP half-width in our population of PV-negative GABAergic neurons was 0.86 ms, and the mean ± SE was 1.24 ± 0.04 ms ($n = 29$) (Fig. 2*D*). Maximal firing rate plotted as a function of AP half-width also indicated two separate classes of GABAergic neurons (Fig. 2*E*). Therefore, there are clear differences between the three classes of layer 2/3 neurons (excitatory, FS GABAergic, and NFS GABAergic neurons) that we have differentiated in this study on the basis of GFP labeling, electrophysiology, anatomy, and PV expression.

Optogenetic stimulation of excitatory layer 2/3 neurons. Our next goal was to investigate the synaptic interactions between these three classes of layer 2/3 neurons. Under our in vitro

brain slice recording conditions, the mean V_m of all classes of neurons were hyperpolarized with respect to AP threshold. Additional excitation is therefore needed to drive neuronal network activity. To stimulate a population of excitatory layer 2/3 neurons, we expressed the light-gated cation channel ChR2 (Boyden et al. 2005; Nagel et al. 2003) as an mCherry fusion protein from a lentivirus under the control of the αCaMKII promoter (Zhang et al. 2007) (Fig. 3*A*). Injection of ~80 nl of this lentivector into layer 2/3 mouse barrel cortex resulted in highly localized expression (Fig. 3*B*) (Aronoff and Petersen 2008; Mateo et al. 2011). Three-dimensional analysis of ChR2-mCherry expression in brain slices of 14 mice revealed that a total of 336 ± 59 neurons were transduced per animal, ranging across different mice from 120 to 908 ChR2-expressing neurons (Fig. 3*C*). With injection sites aligned at their centers, the mean spatial density of ChR2-expressing neurons followed a near-Gaussian profile with a full-width at half-maximal amplitude of 109 μm horizontally along the *x*-axis (lateral dimension within layer 2/3) and 166 μm vertically along the *y*-axis (dimension along the radial column of layers 1–6) (Fig. 3*D*). ChR2-expressing neurons were not found in layer 4, probably because the αCaMKII promoter is relatively inactive in this layer (Nathanson et al. 2009). Within a given injection site, there was a large variance in fluorescence brightness across the population of transduced cells, indicating that ChR2-mCherry was not expressed at uniform levels. Neurons in the center of the injection site generally expressed ChR2-mCherry at higher levels than neurons toward the edge. Differing expression levels will likely lead to variation in light sensitivity across the population of expressing neurons.

To characterize the number of ChR2-expressing neurons that fired APs under our experimental conditions, we sequentially made cell-attached recordings from many neurons distributed across the horizontal and vertical extent of the injection site and recorded their response to wide-field blue light stimulation (3 ms) (Fig. 3*D*). Of 224 extracellular recordings across 6 injection sites, 95 neurons fired with 100% reliability and 129 never fired any APs in response to blue light stimulation. Thus

Table 1. *Intrinsic electrophysiological properties of EXC, FS GABAergic, and NFS GABAergic neurons in L2/3 of mouse barrel cortex*

Properties	EXC	FS	NFS
Resting V_m, mV	−68.1 ± 0.7	−67.5 ± 0.6	−62.6 ± 0.6
R_{in}, MΩ	160 ± 6	99 ± 3	208 ± 7
Rheobase, pA	113 ± 7	208 ± 17	85 ± 9
AP half-width, ms	2.23 ± 0.05	0.57 ± 0.01	1.29 ± 0.03
AP threshold, mV	−37.9 ± 0.3	−37.4 ± 0.4	−36.3 ± 0.4
τ, ms	28.4 ± 0.9	9.3 ± 0.3	21.2 ± 1.3
Maximal AP rate, Hz	18.0 ± 1.2	185 ± 10	47.2 ± 2.5

Data are means ± SE of properties in excitatory (EXC), fast-spiking (FS) GABAergic, and non-fast-spiking (NFS) GABAergic neurons in layer 2/3 (L2/3) of mouse barrel cortex. V_m, membrane potential; R_{in}, input resistance; AP, action potential; τ, membrane time constant.

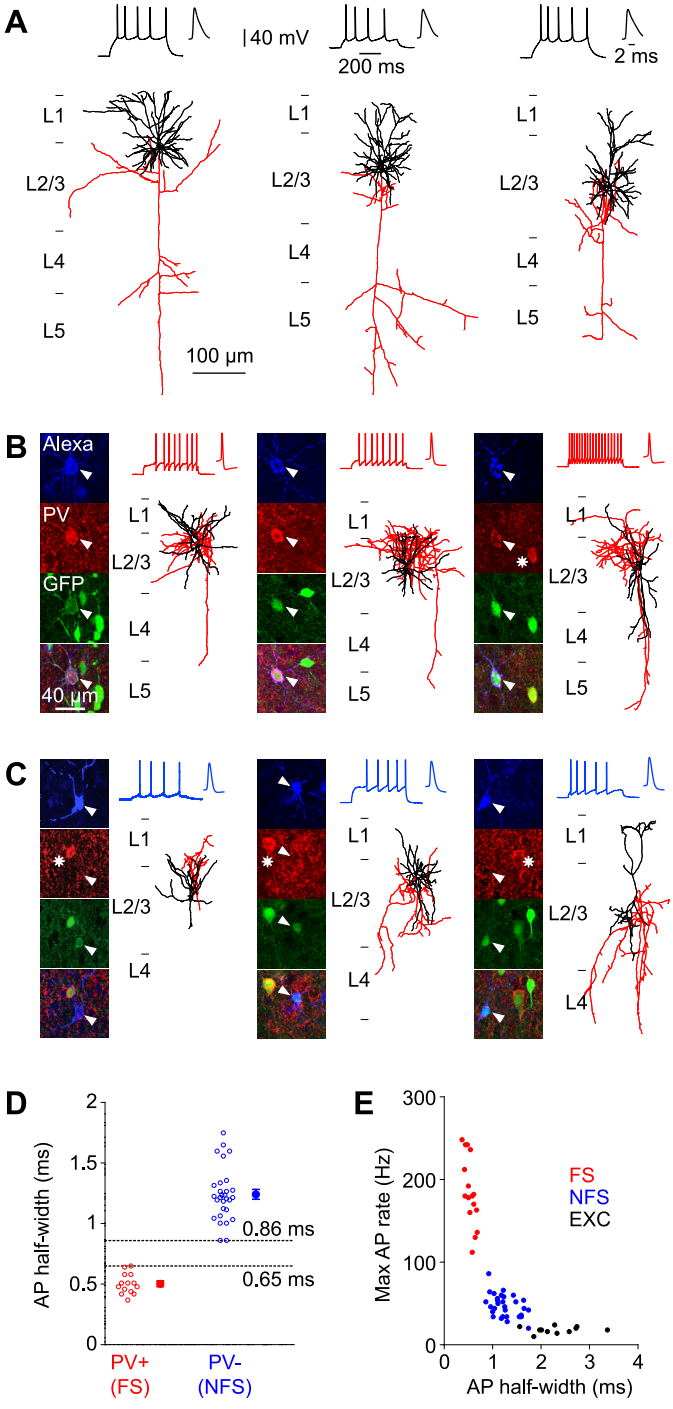

Fig. 2. Anatomical features and parvalbumin (PV) expression of neurons in L2/3 mouse barrel cortex. *A*: 3 example EXC neurons with adapting firing patterns (*top* traces) and broad APs (*insets, top* traces). Dendrites are shown in black and axons in red (*bottom*). Note the long descending axons, which typically send off collaterals in layers 2, 3, and 5 before projecting to their long-range targets. *B*: 3 example FS GABAergic neurons with narrow AP waveforms and little adaptation in their firing patterns (*top* traces). Anatomical reconstructions (*bottom*) indicate dense axon (red) and simple dendrites (black). Fluorescence images show Alexa staining of biocytin-filled neurons (blue), PV immunohistochemistry (red), and GFP (green). All tested FS GABAergic neurons expressed PV. Arrowheads indicate somata of recorded neurons. Asterisk indicates a further PV-positive soma in the same optical plane. *C*: 3 example NFS GABAergic neurons with broad AP waveforms (*top* traces). Immunohistochemistry showed that NFS GABAergic neurons did not express PV. Arrowheads indicate somata of recorded neurons. Asterisks indicate PV-positive somata of other nearby neurons in the same optical plane. *D*: all tested FS GABAergic neurons expressed PV (PV+; $n = 14$; mean AP half-width 0.50 ± 0.02 ms; maximum 0.65 ms). None of the tested NFS GABAergic neurons expressed PV (PV−; $n = 29$; mean AP half-width 1.24 ± 0.04 ms; minimum 0.86 ms). *E*: maximal firing frequency vs. AP half-width.

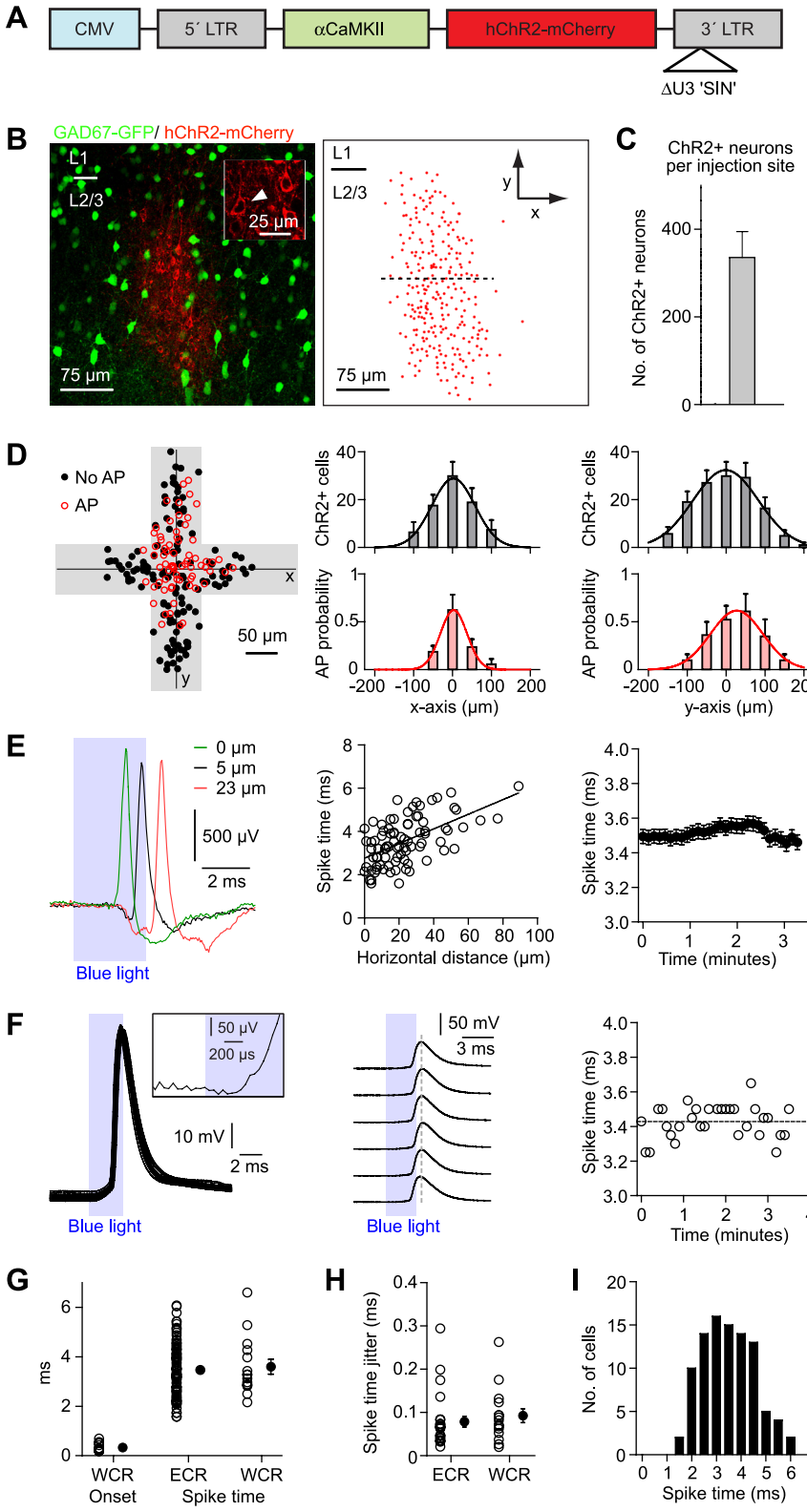

Fig. 3. Optogenetic stimulation of EXC L2/3 neurons. *A*: lentiviral vector construct encoding channelrhodopsin-2-mCherry fusion protein (hChR2-mCherry) under the control of an αCaMKII promoter. LTR, long terminal repeat; SIN, self-inactivating. *B*: confocal image showing expression of ChR2-mCherry 9 days after stereotactic virus injection. Somata of ChR2-expressing (ChR2+) EXC neurons were exclusively localized to L2/3 close to the injection site (*left*). Arrowhead (*inset*) indicates a ChR2-expressing soma. Counts of ChR2-mCherry expressing cells are shown for the same injection site (*right*; red dots indicate location of counted ChR2-expressing somata; $n = 264$ expressing neurons). *C*: average number of ChR2-expressing neurons per brain slice (336 ± 60 cells, $n = 14$ mice). *D*: the number of neurons per injection site spiking in response to blue light stimulation was estimated by making extracellular cell-attached recordings from many neurons along the horizontal and vertical axes of the ChR2 injection site (*left*; red circles indicate location of spiking neurons; black dots indicate nonspiking neurons; $n = 6$ mice). Spatial distributions of total number of ChR2-expressing neurons (*top*) and light-evoked spiking probability (*bottom*) in horizontal (*x*-axis, lateral dimension within L2/3; *center*) and vertical directions (*y*-axis, cortical column dimension; *right*). *E*: example extracellular recordings from 3 different neurons of APs evoked by 3-ms blue light stimulation in the presence of 6-cyano-7-nitroquinoxaline-2,3-dione (CNQX) and D-2-amino-5-phosphonovaleric acid (D-APV) (*left*). Spike latency increased with distance of expressing neuron from center of the injection site (green trace corresponds to a neuron at 0 μm from the center of the injection site with an AP latency of 2.1 ms; black trace represents a neuron at 5 μm from the center of the injection site with an AP latency of 2.8 ms; and red trace shows a neuron located 23 μm from the center of the injection site with a latency of 3.7 ms). Measured across many neurons, AP peak latencies increased as a function of horizontal distance from the center of the injection site (*center*; $n = 95$, $r = 0.53$, $P < 0.0001$). AP peak latencies were stable over time (*right*; $n = 25$ cells). *F*: example whole cell recording of a ChR2-expressing EXC neuron. AP firing was evoked by blue light stimulation with high temporal precision and low jitter (black traces; mean AP peak time 3.43 ± 0.02 ms). *Inset* shows rapid onset of ChR2-triggered depolarization (onset latency 350 μs). *G*: onset latency of ChR2-expressing cells for ChR2-evoked depolarization (whole cell recordings; WCR onset) compared with mean spike time in WCR and in extracellular cell-attached recordings (ECR). *H*: ChR2-evoked AP firing occurred with low temporal jitter in both WCR and ECR. *I*: spike time distribution of ChR2-evoked AP firing computed across all recordings indicates a near-synchronous stimulation. Data are means ± SE.

the population of neurons firing an AP in response to the optogenetic stimulation showed low trial-to-trial variability. Aligned to the center of the injection site, the mean spatial distribution of light-evoked AP firing followed a near-Gaussian distribution with a full-width at half-maximal probability of 67 μm horizontally and 132 μm vertically (Fig. 3*D*). The spatial extent of spiking neurons is therefore smaller than the spatial extent of ChR2-expressing neurons, presumably because the expression levels drop toward the edges of the injection site. Assuming rotational symmetry around the cortical column axis (which we denote as the *y*-axis, with the *x*-axis representing horizontal lateral space), we can estimate the approximate total

number of spiking neurons as $(R_x)^2 \times R_y \times n$, where R_x and R_y are the ratios of spatial width of spiking cells with respect to the spatial width of ChR2-expressing cells, and n is the average number of ChR2-expressing neurons per injection site (R_x = 0.61, R_y = 0.80, n = 336 with a range of 120–908, giving a mean total estimate of 101 spiking neurons with a range of 36–273). This number of spiking neurons is likely to be an overestimate, since blue light penetration deep into the brain slice is likely to be impaired by the strong light scattering of neural tissue.

AP latency varied with distance from the center of the injection site, presumably also correlating with ChR2 expression levels. At the center of the injection site, a large fraction of neurons reliably fired APs at short latency with little jitter in response to the blue light pulse (Fig. 3*E*), but toward the edge of the injection site only very few neurons were driven to fire APs, and these occurred after a longer latency (Fig. 3*E*).

Whole cell recordings from ChR2-expressing neurons (Fig. 3*F*) indicated that depolarization began rapidly after onset of blue light illumination with a latency of 0.33 ± 0.04 ms (n = 15) (Fig. 3*G*). AP latency measured in whole cell recordings was 3.6 ± 0.3 ms (n = 15), and AP latency from extracellular measurements was 3.5 ± 0.1 ms (n = 95) (Fig. 3*G*). Jitter in AP timing was low in both whole cell (0.09 ± 0.02 ms, n = 15) and extracellular recordings (0.08 ± 0.01 ms, n = 25) (Fig. 3*H*). Across the population of recorded neurons, light-evoked AP firing in ChR2-expressing neurons occurred near-synchronously within a relatively narrow time window from 1 to 6 ms after blue light onset (Fig. 3*I*).

Rapid recruitment of inhibition by the excitatory optogenetic stimulus. Whole cell membrane potential recordings from postsynaptic excitatory neurons that did not express ChR2 (Fig. 4*A*) revealed that the optogenetic stimulus synaptically drives a reliable and brief depolarization after a short latency (PSP peak amplitude, 2.4 ± 0.7 mV; PSP onset latency, 4.7 ± 0.3 ms; n = 23 excitatory neurons). This is consistent with optogenetic stimulation of excitatory neurons releasing glutamate onto synaptically coupled postsynaptic target neurons, opening ionotropic glutamate receptors to generate an excitatory postsynaptic potential (EPSP). However, depolarizing the postsynaptic neuron by somatic current injection revealed that powerful inhibition rapidly follows the excitatory input (Fig. 4*B*). The application of CNQX and APV (to block AMPA- and NMDA-type ionotropic glutamate receptors, respectively) completely abolished the light-evoked response at both resting and depolarized membrane potentials (n = 5 cells recorded in 5 slices from 5 different mice) (Fig. 4*B*). The hyperpolarizing response recorded at depolarized potentials could be completely blocked by picrotoxin (a $GABA_A$ receptor antagonist; n = 9 cells recorded in 9 slices from 9 mice). Because of the long washout period of CNQX/APV of ~1 h, sequential application of CNQX/APV followed by picrotoxin in the same recording was only successfully carried out for two cells (Fig. 4*B*). These results reveal that the GABAergic inhibition is disynaptic and functionally confirm the specific expression of ChR2 in excitatory neurons.

To study the time course of the recruited disynaptic inhibition, we computed time-dependent reversal potentials of the light-evoked postsynaptic response by injecting different current levels into the recorded neuron (Fig. 4*C*). Because AP firing at depolarized membrane potentials disturbs measurement of synaptic potentials, we only tested a small range of subthreshold potentials and then extrapolated linear fits to the data to obtain reversal potentials. The extrapolation will inevitably add error to our estimates of reversal potential. The early optogenetically evoked response was driven mainly by excitatory conductances (reversal potential was −17.1 ± 7.6 mV, n = 9; measured on the rising phase of the PSP at half-maximal amplitude, 8.3 ± 0.6 ms after blue light stimulus onset). However, within a few milliseconds inhibition began to dominate (reversal potential was −45.1 ± 3.3 mV, n = 9; measured at the time of the PSP peak amplitude, 15.4 ± 1.2 ms after blue light stimulus onset) and the reversal potential stayed hyperpolarized for the remainder of the PSP (at 35 ms following light onset, reversal potential was −52.4 ± 3.0 mV, n = 9) (Fig. 4, *C* and *D*). We therefore conclude that the optogenetic stimulus of layer 2/3 excitatory glutamatergic neurons evokes synaptically driven AP firing in GABAergic neurons, mediating rapid disynaptic inhibition. To understand how such disynaptic inhibition was recruited by the optogenetic stimulus, we recorded the light-evoked membrane potential responses in GFP-labeled layer 2/3 GABAergic neurons.

Simultaneous and sequential whole cell recordings were made from different classes of postsynaptic neurons near the ChR2-mCherry injection site (distance from center of injection site: excitatory neurons, 124 ± 40 μm, n = 35; FS GABAergic neurons, 111 ± 50 μm, n = 55; NFS GABAergic neurons, 118 ± 48 μm, n = 44). In any individual experiment, the amplitude of the depolarizing PSP was usually larger in FS GABAergic neurons compared with excitatory and NFS GABAergic neurons (example experiment shown in Fig. 5*A*). Analyzed across all experiments, we found that FS GABAergic neurons had significantly larger PSP amplitudes compared with excitatory neurons (Fig. 5*B*). FS GABAergic neurons also had significantly larger PSP slopes compared with both excitatory and NFS GABAergic cells (Fig. 5*C*). Most importantly, FS GABAergic neurons fired synaptically driven APs with much higher probability than excitatory or NFS GABAergic neurons (postsynaptic cells firing APs: 0 of 35 excitatory neurons, 10 of 55 FS GABAergic neurons, and 1 of 44 NFS GABAergic neurons) (Fig. 5, *A* and *D*). PSP onset latency was shorter in GABAergic neurons compared with excitatory neurons (Fig. 5*E*). The duration of the evoked PSP was shortest in FS GABAergic neurons (Fig. 5*F*). The rise time of the PSP was fastest in FS GABAergic neurons (Fig. 5*G*).

Part of the variability in PSP amplitude across different recordings likely results from variability in the number of ChR2-expressing neurons in different brain slices. Because responses were largest in FS GABAergic neurons, we further analyzed experiments in which at least one of the recorded cells was a FS GABAergic neuron. The grand average PSP time courses of these experiments show that FS GABAergic neurons had larger and faster responses compared with excitatory and NFS GABAergic neurons (Fig. 5*H*). The peak PSP amplitude was 5.3 ± 1.0 mV in FS GABAergic neurons (n = 37), 1.9 ± 0.4 mV in NFS GABAergic neurons (n = 34), and 1.5 ± 0.5 mV in excitatory neurons (n = 25) (Fig. 5*I*). Note that measurements of PSP amplitude can only be made from nonspiking neurons, and therefore the PSP amplitude reported for FS GABAergic neurons is underestimated. Normalizing the average PSP amplitudes within each individual experiment to the amplitude of the mean subthreshold response of the FS

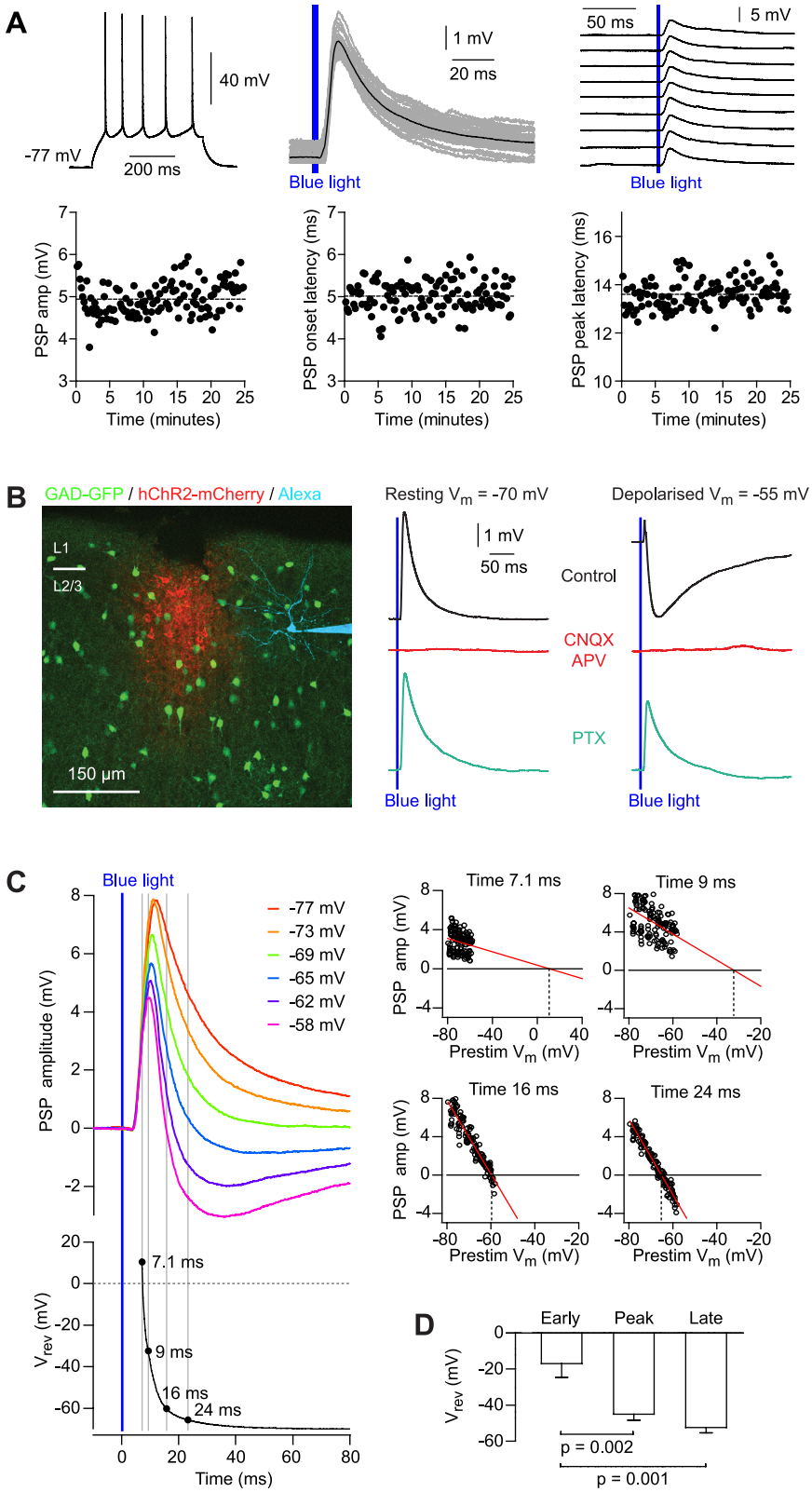

Fig. 4. Postsynaptic response indicates recruitment of disynaptic inhibition by the excitatory optogenetic stimulus. *A*: firing pattern (*top left*) and example optogenetically evoked postsynaptic responses recorded in a ChR2-nonexpressing excitatory neuron (*top center* and *top right*). ChR2-evoked postsynaptic potentials (PSPs) were reliably triggered across 125 trials over 25 min (graphs at *bottom*; dashed lines indicate mean values: PSP amplitude 4.94 ± 0.02 mV, PSP onset latency 5.02 ± 0.03 ms, PSP peak latency 13.60 ± 0.05 ms). *B*: superimposed images (*left*) of ChR2-expressing cells in L2/3 (red), the recorded postsynaptic excitatory cell (blue), and GFP-labeled GABAergic neurons (green). In this example experiment, blue light ChR2 stimulation evoked a depolarizing PSP at the resting V_m of −70 mV (black trace, *center*) that was entirely blocked by application of CNQX and D-APV (red trace, *center*). After washout of these ionotropic glutamate receptor antagonists, picrotoxin (PTX) was added to block $GABA_A$ receptors, which lengthened the duration of the PSP (blue trace, *center*). Depolarization of the postsynaptic neuron to −55 mV by current injection (*right*) revealed that the optogenetic stimulus in fact first evoked excitation, which was rapidly followed by inhibition (black trace, *right*). Both parts of the response were completely blocked by application of CNQX and APV (red trace, *right*). Only the hyperpolarizing PSP was blocked by PTX (blue trace, *right*). *C*: the postsynaptic response evoked by optogenetic stimulation in this example experiment was recorded at many different potentials (*top left*). The time-dependent reversal potential (V_{rev}) of the ChR2-evoked PSP was computed (200 time points over 80 ms). At 7.1 ms (*top center*, the earliest time point at which V_{rev} could reliably be computed; $P < 0.05$; $r > 0.15$), V_{rev} was depolarized (10.4 mV). Two ms later (*top right*), V_{rev} was more hyperpolarized (−32.3 mV), indicating a rapid onset of inhibitory conductances. The 2 apparent clusters of data points observed at 7.1 ms and 9 ms might reflect timing differences in the recruitment of a powerful GABAergic neuron varying across trials, giving trial-to-trial variability in response amplitude. For the remainder of the PSP, V_{rev} remained hyperpolarized (V_{rev} minimum = −70.0 mV). *D*: computed across 9 recordings, the average V_{rev} was dominated by excitatory conductances at early time points (at half-maximal PSP amplitude on the rising phase), but at the PSP peak time and at a late time (35 ms after blue light onset), inhibitory conductances dominated. Data are means ± SE.

GABAergic neurons recorded in that slice, we found that NFS GABAergic neurons received significantly larger PSPs than excitatory neurons (Fig. 5*J*). Relative to FS GABAergic neurons, the PSP amplitude ratio for excitatory neurons was 0.21 ± 0.05 (EXC/FS; n = 19), and for NFS GABAergic neurons the ratio was 0.37 ± 0.06 (NFS/FS; n = 15) (Fig. 5*J*). If these ratios are renormalized to the PSP amplitude measured in excitatory neurons, the ratio of excitatory synaptic input onto our three classes of postsynaptic neurons (excitatory/NFS/FS) is 1:1.8:4.8.

These experiments reveal that the near-synchronous optogenetic stimulation of a relatively small, localized population of excitatory layer 2/3 neurons drives depolarization in all classes of nearby postsynaptic neurons, with the largest responses in FS GABAergic neurons. Postsynaptic spiking activity in FS GABAergic cells appears to be the key neuronal population driving disynaptic inhibition under these experimental conditions.

Unitary synaptic connectivity of excitatory and inhibitory layer 2/3 neurons of mouse barrel cortex. To examine the synaptic mechanisms driving these network interactions, we investigated the local unitary synaptic connectivity of excitatory and inhibitory layer 2/3 neurons through multiple simultaneous whole cell recordings of nearby neurons (somata separation: 61 ± 39 μm, mean ± SD; n = 357 pairs) (Fig. 6,

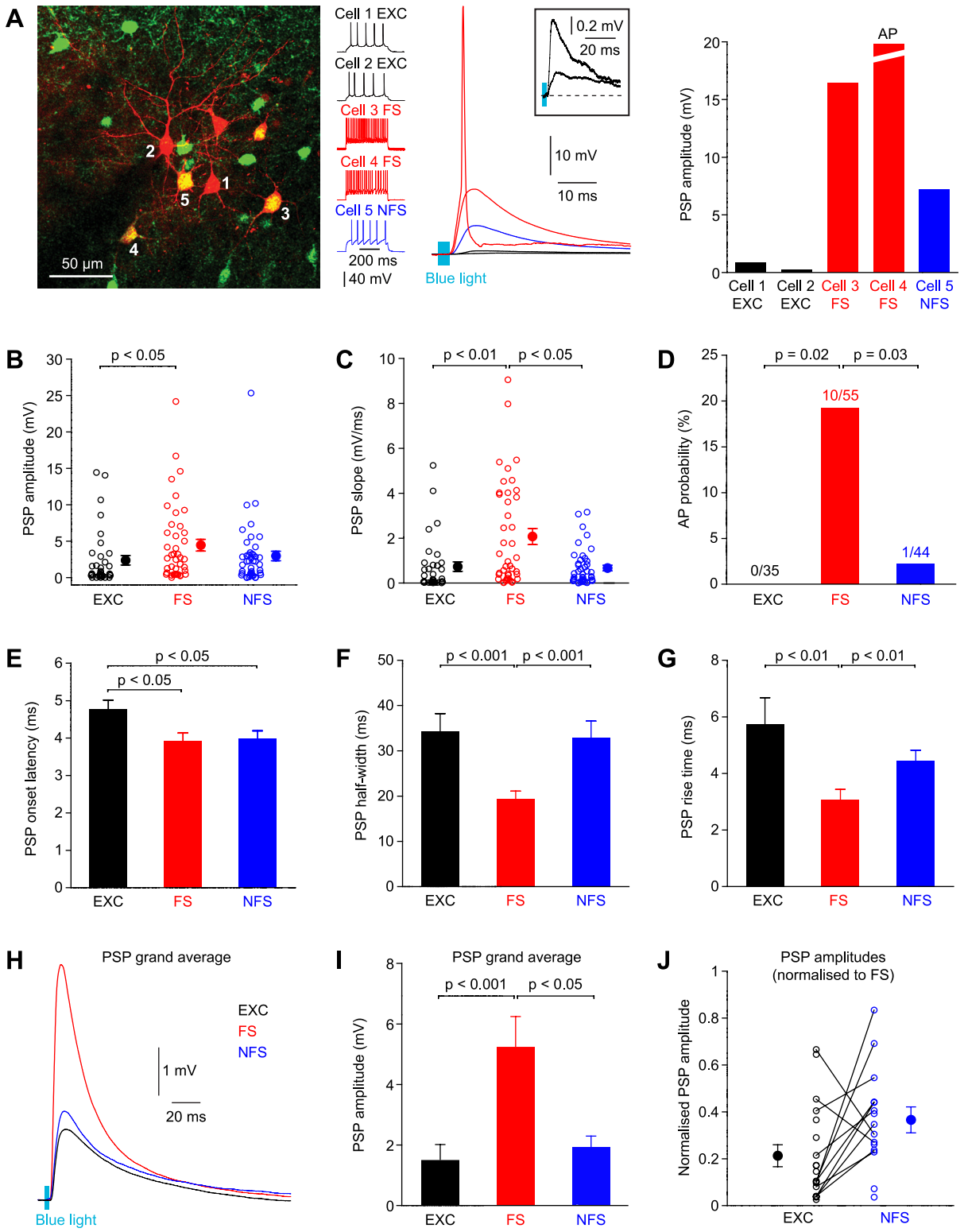

A and *B*). Synaptic connectivity was tested by injecting a brief depolarizing current pulse to evoke an AP in the presynaptic neuron while simultaneously recording the membrane potential in putative postsynaptic target neurons. When presynaptic excitatory neurons were stimulated, the putative postsynaptic neurons were recorded at resting membrane potential. When presynaptic inhibitory neurons were stimulated, the postsynaptic neurons were depolarized to −55 mV to enhance the electrochemical driving force for chloride influx through $GABA_A$ receptors. Across a large number of recordings, we found that excitatory neurons made synaptic connections with significantly higher probability onto FS GABAergic neurons than onto excitatory or NFS GABAergic neurons ($P_{EXC\rightarrow EXC}$ = 17%, $P_{EXC\rightarrow FS}$ = 58%, $P_{EXC\rightarrow NFS}$ = 24%) (Fig. 6*C* and Table 2). Action potentials in excitatory neurons also evoked significantly larger-amplitude unitary excitatory postsynaptic potentials (uEPSPs) in FS GABAergic neurons compared with NFS GABAergic neurons and excitatory neurons ($uEPSP_{EXC->EXC}$ = 0.37 ± 0.10 mV; $uEPSP_{EXC->FS}$ = 0.82 ± 0.10 mV; $uEPSP_{EXC->NFS}$ = 0.39 ± 0.11 mV) (Fig. 6*C* and Table 2). The uEPSP kinetics were faster in FS GABAergic neurons having shorter latency, faster rise time, and shorter duration than in excitatory and GABAergic NFS neurons (Fig. 6, *E* and *F*, and Table 3).

Both FS GABAergic neurons and NFS GABAergic neurons had strong inhibitory synaptic connectivity with nearby neurons (Fig. 6, *C* and *D*, and Table 2). Unitary inhibitory postsynaptic potentials (uIPSPs) in excitatory neurons originating from presynaptic FS GABAergic neurons had shorter latencies, faster rise times, and shorter durations compared with those originating from NFS GABAergic neurons (Fig. 6, *E* and *F*, and Table 3). This is consistent with the notion that PV-expressing FS GABAergic neurons preferentially innervate electrotonically proximal neurites of excitatory neurons, with some FS neurons innervating soma and proximal dendrites (Bartos et al. 2007; Freund and Katona 2007) and other FS neurons innervating the axon initial segment (Somogyi 1977). The slower uIPSPs originating from presynaptic NFS GABAergic neurons might indicate that they preferentially innervate more distal regions of the dendritic arborizations of excitatory postsynaptic neurons, although other mechanisms such as slower AP conduction, differences in rate of neurotransmitter release, and kinetics of different types of postsynaptic $GABA_A$ receptors may also contribute to the slower inhibition evoked by NFS GABAergic neurons. Inhibitory synaptic connections from FS GABAergic onto NFS GABAergic neurons occurred at significantly lower probability than inhibitory connections from FS GABAergic neurons onto excitatory neurons or other FS GABAergic neurons ($P_{FS\rightarrow EXC}$ = 60%, $P_{FS\rightarrow FS}$ = 55%, $P_{FS\rightarrow NFS}$ = 24%) (Fig. 6*C* and Table 2). There were no significant differences when the inhibitory synaptic connectivity of presynaptic NFS GABAergic neurons onto different classes of postsynaptic targets was compared ($P_{NFS\rightarrow EXC}$ = 47%, $P_{NFS\rightarrow FS}$ = 38%, $P_{NFS\rightarrow NFS}$ = 38%) (Fig. 6*C* and Table 2). Electrical coupling, presumably through gap junctions, was observed in 8 of 12 pairs of GABAergic FS neurons with a steady-state coupling coefficient of 3.3 ± 0.6% (n = 8) (Galarreta and Hestrin 1999; Gibson et al. 1999), but we did not find electrical coupling between GABAergic FS and NFS neurons (0 of 21 pairs) or between pairs of GABAergic NFS neurons (0 of 8 pairs).

We examined the dependence of synaptic connectivity on the intersomatic distance of the recorded neurons, but over the small length scale tested (<150 μm), there was no significant change in the probability of finding connections for any of the classes of synaptic connections we analyzed in layer 2/3 (Fig. 7*A*), in agreement with a previous study of connectivity among excitatory neurons in mouse barrel cortex (Lefort et al. 2009).

Nonrandom higher order patterns of synaptic connectivity have been reported for several classes of synaptic connections in the neocortex (Brown and Hestrin 2009; Kampa et al. 2006; Ko et al. 2011; Markram et al. 1997; Perin et al. 2011; Song et al. 2005; Yoshimura et al. 2005). The simplest higher order structure in synaptic connectivity would be an above chance level of finding reciprocally connected pairs of neurons. Such enhancement of reciprocal connections is predicted for neuronal networks operating with rate coding, but not for temporal coding (Clopath et al. 2010). In agreement with a previous analysis of synaptic connectivity limited to excitatory neurons of mouse barrel cortex (Lefort et al. 2009), we did not find evidence for any significant enhancement of finding bidirectionally synaptically coupled pairs above chance level among any of our neuronal classes (Fig. 7*B* and Table 4). Equally, the unitary PSP amplitudes were not different when unidirectionally and bidirectionally synaptically coupled pairs of neurons were compared (Fig. 7*C*). However, note that large sample size is typically necessary to detect higher order patterns of connectivity, and in our limited data set we can only define broad confidence intervals compatible with random reciprocity (Table 4). Larger data sets would narrow the confidence intervals, perhaps allowing nonrandom patterns of reciprocity to be resolved.

Computational modeling of the layer 2/3 neuronal network. We made simple computational models of spiking neuronal networks (Gerstner and Kistler 2002) to assess to what extent our unitary connectivity data were able to account for the network activity evoked by optogenetic stimulation of excitatory neurons. We used the experimentally determined distribution of intrinsic electrophysiological properties (V_m, AP

Fig. 5. Optogenetic stimulation evoked larger amplitude PSPs in FS GABAergic neurons, which were also more likely to fire synaptically driven APs compared with EXC and NFS GABAergic neurons. *A*: example experiment showing recordings from 2 EXC and 3 GABAergic L2/3 neurons responding differentially to ChR2-driven glutamatergic excitation (*far left*, 2-photon image stack; *center left*, firing patterns; *center right*, membrane potential evoked by blue light stimulation, with *inset* showing response in excitatory neurons on an expanded scale; *far right*, quantification of peak PSP amplitudes). PSPs in FS GABAergic neurons were larger than responses in excitatory or NFS GABAergic neurons. One of the FS GABAergic neurons (*cell 4*) reliably fired an AP in response to the optogenetic stimulus. *B*: peak amplitudes of PSPs evoked by ChR2 stimulation across cell types. Postsynaptic neurons that fired APs were not included in this analysis. *C*: slopes of ChR2-evoked PSPs. *D*: fraction of cells firing synaptically driven APs. *E*: ChR2-evoked PSP onset latencies. *F*: half-width of ChR2-evoked PSPs. *G*: ChR2-evoked PSP rise time (20–80%). *H*: grand average time course of ChR2-evoked PSPs across all experiments in which at least 1 recording was from a FS GABAergic neuron. *I*: grand average PSP amplitudes across all experiments in which at least 1 recording was from a FS GABAergic neuron. *J*: PSP amplitudes normalized within each experiment to the mean response found in FS GABAergic neurons in the same slice. Each circle represents the PSP ratio per experiment and cell type. Lines indicate data from the same experiment. Data are means ± SE.

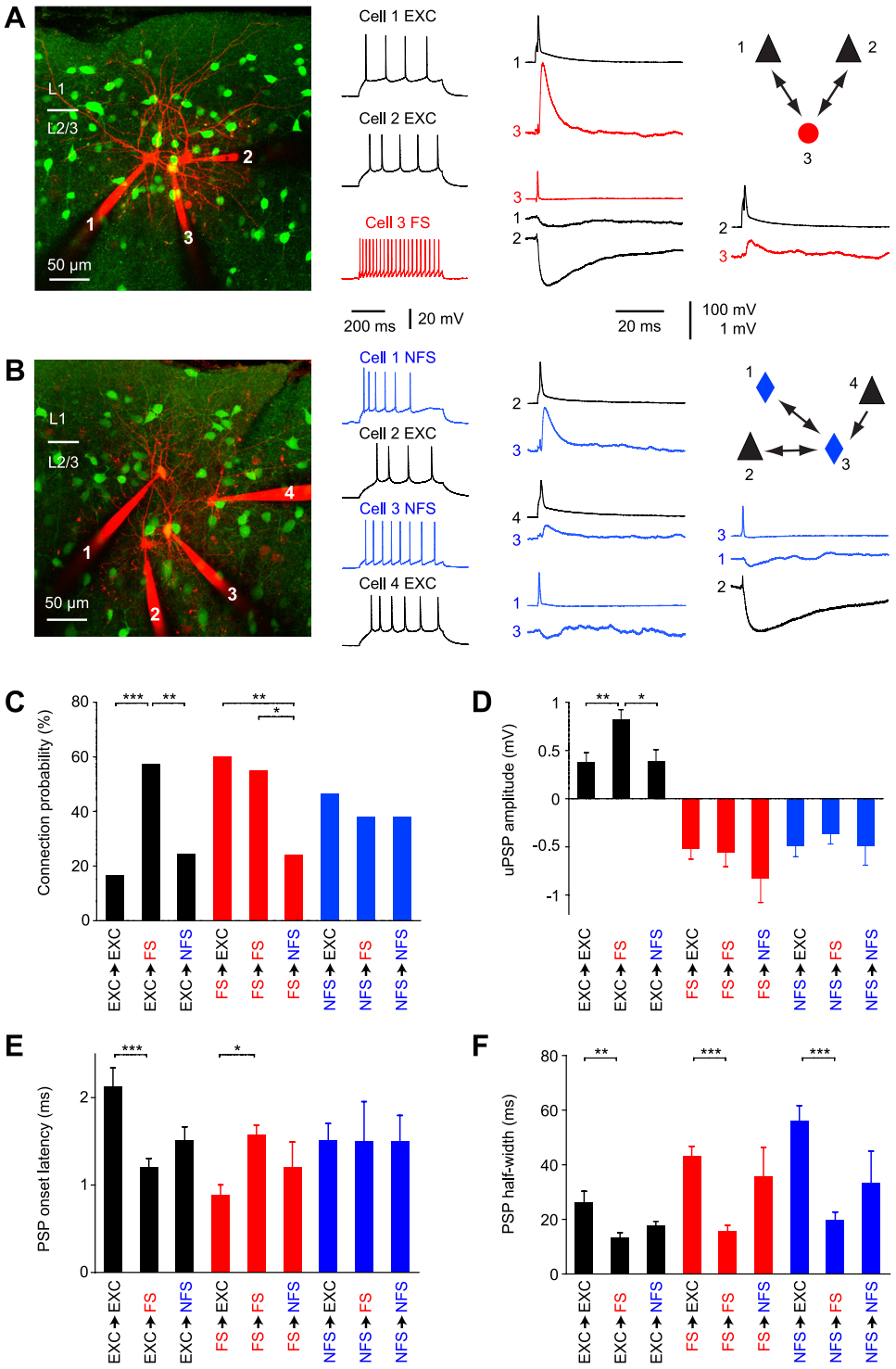

Fig. 6. Analysis of unitary synaptic connections. *A*: example recording testing for synaptic connectivity between 2 EXC neurons and 1 FS GABAergic neuron. An AP driven by current injection into either of the EXC neurons (*cell 1* or *cell 2*) evoked a unitary excitatory PSP in the FS GABAergic neuron (*cell 3*). Conversely, an AP in the FS GABAergic neuron evoked a unitary inhibitory PSP (measured at −55 mV) in both EXC neurons (*cell 1* and *cell 2*). Both EXC neurons were therefore bidirectionally coupled to the FS GABAergic neuron. The 2 EXC neurons were not synaptically connected to each other (not shown). *B*: example recording probing synaptic connectivity between 2 EXC neurons and 2 NFS GABAergic neurons. Both EXC neurons (*cell 2* and *cell 4*) provide synaptic input to 1 of the NFS GABAergic neurons (*cell 3*), which also inhibits 1 of the EXC neurons (*cell 2*). The 2 NFS GABAergic neurons (*cell 1* and *cell 3*) reciprocally inhibit each other. *C*: probabilities of finding synaptically coupled pairs of neurons among the 3 different neuron classes. *D*: amplitudes of unitary synaptic connections among the 3 different neuron classes. *E*: PSP onset latencies of unitary synaptic connections among the 3 different neuron classes. *F*: PSP duration of unitary synaptic connections among the 3 different neuron classes. Data are means ± SE. $*P < 0.05$; $**P < 0.01$; $***P < 0.001$, statistically significant differences of PSP amplitudes, latencies and durations were assessed by nonparametric Kruskal-Wallis test followed by Dunn's posttest. Significant differences in connectivity were tested with a χ^2 statistic on contingency table.

threshold, τ, and R_{in}; Table 1) and the experimentally determined distribution of unitary synaptic connectivity (uPSP amplitudes, kinetics, and connection probabilities; Tables 2 and 3) to construct a simplified adaptive exponential (AdEx) integrate-and-fire model (Brette and Gerstner 2005) of the layer 2/3 neuronal network containing the appropriate number of class-specific neurons for a single cortical barrel column (Gentet et al. 2010; Lefort et al. 2009) (Fig. 8).

Stimulation of a single excitatory layer 2/3 pyramidal neuron in the computational model evoked uEPSPs in postsynaptic neurons with a mean ± SD amplitude averaged across all neurons (both synaptically connected and unconnected) of a given cell type of 0.066 ± 0.005 mV in excitatory neurons, 0.55 ± 0.08 mV in FS GABAergic neurons, and 0.10 ± 0.02 mV in NFS GABAergic neurons (Fig. 8*A*). No APs were fired in postsynaptic layer 2/3 neurons in response to the stimulation of a single excitatory neuron. If a single excitatory neuron was depolarized to −55 mV, then the amplitude of the evoked PSP was slightly smaller compared with the response evoked from resting membrane potential due to a

Table 2. *Synaptic connectivity and uPSP amplitudes in L2/3 of mouse barrel cortex*

Postsynaptic	Presynaptic EXC	Presynaptic FS	Presynaptic NFS
EXC			
P, % (found/tested)	16.8% (16/95)	60.0% (21/35)	46.5% (20/43)
Mean ± SE, mV	0.37 ± 0.10	−0.52 ± 0.11	−0.49 ± 0.11
Median, mV	0.20	−0.29	−0.30
Range, mV	0.06–1.42	−0.10 to −1.55	−0.10 to −2.00
FS			
P, % (found/tested)	57.5% (23/40)	55.0% (11/20)	37.9% (11/29)
Mean ± SE, mV	0.82 ± 0.10	−0.56 ± 0.14	−0.37 ± 0.10
Median, mV	0.68	−0.44	−0.23
Range, mV	0.16–1.94	−0.07 to −1.46	−0.12 to −0.99
NFS			
P, % (found/tested)	24.4% (11/45)	24.1% (7/29)	38.1% (8/21)
Mean ± SE, mV	0.39 ± 0.11	−0.83 ± 0.25	−0.49 ± 0.20
Median, mV	0.19	−0.60	−0.15
Range, mV	0.12–1.21	−0.09 to −1.85	−0.07 to −1.47

The probability (*P*) of finding a synaptically connected pair of neurons with somata located in L2/3 is given as a percentage and as the ratio of the number of functional synaptic connections "found" to the number of connections "tested." Unitary postynaptic potential (uPSP) amplitude is given as the mean ± SE, median, and range. According to a nonparametric Kruskal-Wallis test followed by Dunn's posttest, significant differences in uPSP amplitudes were found for EXC-EXC vs. EXC-FS and for EXC-FS vs. EXC-NFS. Significant differences in connectivity were assessed by a χ^2 statistic on contingency table. Differences in excitatory connectivity were found for EXC-EXC vs. EXC-FS and EXC-FS vs. EXC-NFS. Differences in inhibitory connectivity were found for FS-EXC vs. FS-NFS.

reduction in electrochemical driving force for excitatory conductances (Fig. 8*B*).

Increasing the number of simultaneously stimulated excitatory neurons drove larger amplitude PSPs, resulting in substantial recruitment of postsynaptic spiking in FS GABAergic neurons. The stimulation of 50 excitatory neurons synaptically drove APs in 15 ± 2% (mean ± SD) of FS GABAergic neurons, with only 1 ± 1% of NFS GABAergic neurons firing APs and without any AP firing in postsynaptic excitatory neurons (Fig. 8, *C* and *E*). These results are similar to the fraction of spiking postsynaptic cells found experimentally in response to the optogenetic stimulus, where we found 0% firing in excitatory neurons, 18% firing in FS GABAergic neurons, and 2% firing in NFS GABAergic neurons (Fig. 5*D*). However, the PSP amplitudes evoked by stimulating 50 excitatory neurons were considerably larger in the computational model (excitatory: 3.4 ± 0.1 mV; FS: 21.0 ± 0.5 mV; and NFS: 4.8 ± 0.2 mV; means ± SD) (Fig. 8, *C* and *F*) compared with the experimental optogenetic data (excitatory: 1.5 ± 0.5 mV; FS: 5.3 ± 1.0 mV; and NFS: 1.9 ± 0.4 mV; means ± SE). The absolute PSP amplitudes evoked in the model depended strongly on the number of neurons stimulated, which in the optogenetic experiments varied across animals. The ratio of PSP amplitudes across different cell classes is therefore a more reliable indicator for comparing experimental data and the computational model. In the computational model with a stimulus of 50 excitatory neurons, we found a PSP amplitude ratio (normalized to FS GABAergic neurons) for excitatory neurons of EXC/FS = 0.16 and for NFS GABAergic neurons of NFS/FS = 0.23. These ratios from the computer simulation are in relatively close agreement with the in vitro optogenetic experimental data, where we found EXC/FS = 0.21 and NFS/FS = 0.37. When these values were renormalized to the PSP amplitudes in excitatory neurons, we found for the computational model a ratio of EXC/NFS/FS = 1:1.4:6.3 compared with the experimental optogenetic data, which gave a ratio of EXC/NFS/FS = 1:1.8:4.8. Depolarizing the postsynaptic target neuron to −55 mV led to obvious changes in PSP kinetics due to recruitment of disynaptic hyperpolarizing inhibition in response to the stimulation of 50 excitatory neurons (Fig. 8*D*), similar to the results from optogenetic experiments (Fig. 4, *B* and *C*).

As stimulus size increased, a large fraction of FS GABAergic neurons were driven to fire APs, and in addition, the recruitment of NFS GABAergic neurons became more prominent (Fig. 8*E*). When 100 excitatory neurons were stimulated, the computational model predicted postsynaptic spiking in 0.01 ± 0.01% (mean ± SD) of excitatory neurons, 81.1 ± 2.3% of FS GABAergic neurons, and 5.2 ± 1.3% of NFS GABAergic neurons (Fig. 8*E*). For even larger stimuli, the response in FS GABAergic neurons saturated and NFS GABAergic neurons were increasingly also driven to fire APs.

Introducing small amounts of temporal spread in the timing of action potentials in presynaptic neurons affected responses in all types of postsynaptic cells. With an even spread of AP firing across 5 ms in 100 stimulated presynaptic neurons, evoked firing in postsynaptic neurons was reduced to 0.01 ± 0.02% (mean ± SD) of excitatory neurons, 60.6 ± 7.1% of FS GABAergic neurons, and 2.0 ± 0.9% of NFS GABAergic neurons. With an even 10-ms spread of AP firing in 100 presynaptic neurons, evoked firing in postsynaptic neurons was reduced to 0 ± 0% (mean ± SD) of excitatory neurons, 22.4 ± 6.0% of FS GABAergic neurons, and 0.6 ± 0.5% of NFS GABAergic neurons. Even with increased temporal spread in the stimulus, FS neurons dominated the postsynaptic spiking response of the simulated layer 2/3 neuronal network.

Synchronous and near-synchronous activity in excitatory neurons thus rapidly recruits AP firing in postsynaptic FS GABAergic neurons in both the computational model and the experimental data. We next examined the impact of the synaptically evoked AP firing in GABAergic neurons on the responses of the postsynaptic excitatory neurons. In the computational model, we separately turned off the inhibitory syn-

Table 3. *Kinetics of uPSPs*

Postsynaptic	Presynaptic EXC	Presynaptic FS	Presynaptic NFS
Half-width, ms			
EXC	26.2 ± 4.1	43.1 ± 3.7	56.2 ± 5.5
FS	13.7 ± 1.7	15.8 ± 2.0	20.0 ± 2.7
NFS	17.9 ± 1.3	35.7 ± 11	33.3 ± 12
Latency, ms			
EXC	2.1 ± 0.2	0.9 ± 0.1	1.5 ± 0.2
FS	1.2 ± 0.1	1.6 ± 0.1	1.5 ± 0.5
NFS	1.5 ± 0.2	1.2 ± 0.3	1.5 ± 0.3
Rise time, ms			
EXC	3.5 ± 0.6	3.4 ± 0.5	5.4 ± 0.5
FS	1.6 ± 0.2	1.8 ± 0.2	3.1 ± 0.6
NFS	2.6 ± 0.5	2.9 ± 0.5	4.9 ± 1.2
Decay time, ms			
EXC	28.6 ± 4.7	40.0 ± 4.4	52.5 ± 7.3
FS	11.7 ± 1.6	16.4 ± 4.1	16.8 ± 4.1
NFS	16.7 ± 2.2	40.8 ± 15	32.4 ± 12

Values are means ± SE.

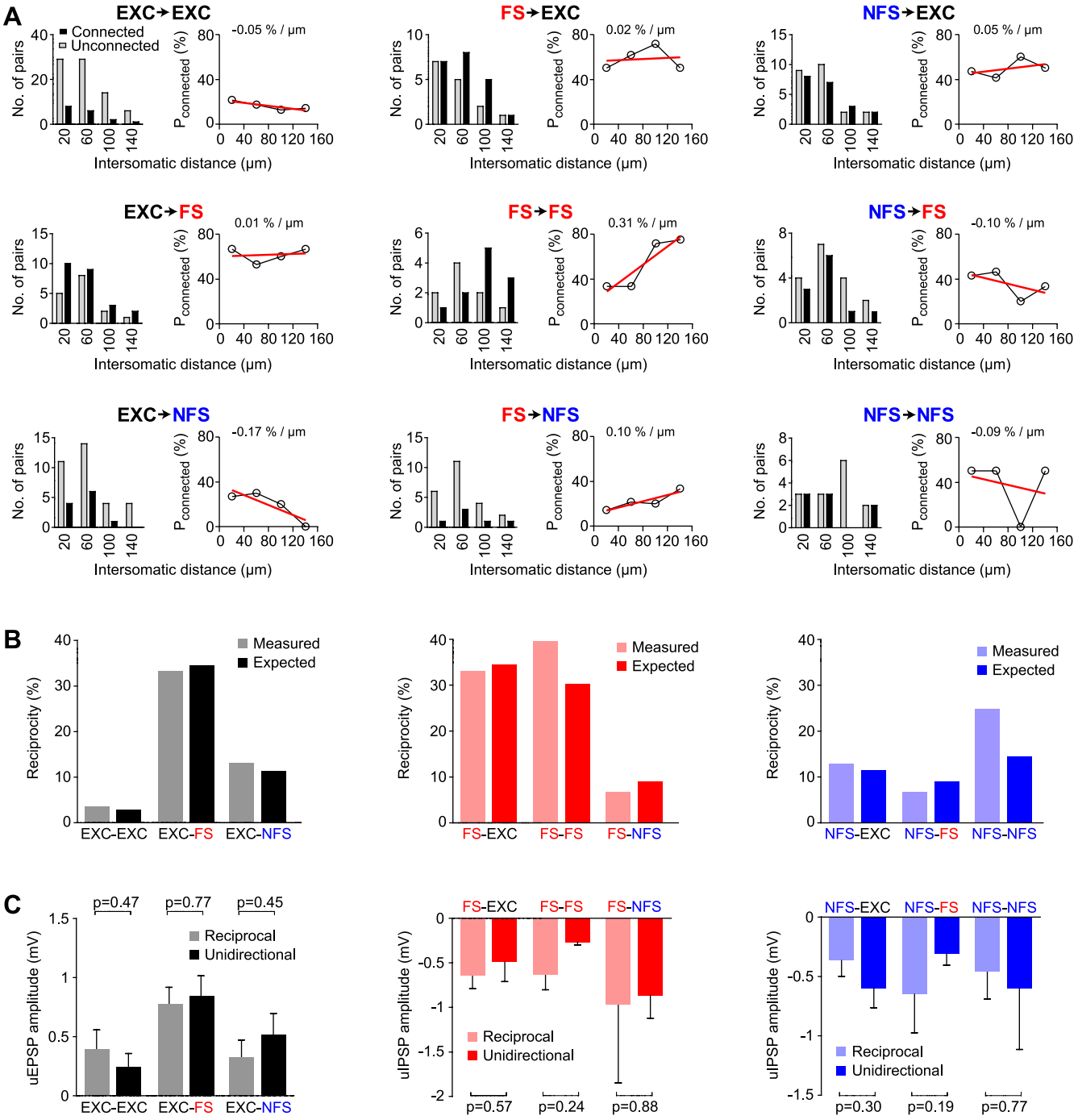

Fig. 7. Spatial extent and reciprocity for excitatory and inhibitory synaptic connections in mouse L2/3 barrel cortex. *A*: for each class of synaptic connection, the intersomatic horizontal distance between both connected and unconnected pairs of neurons is shown (*left*) together with the connection probability as a function of soma separation (*right*; red line shows best linear fit). Synaptic connectivity was not dependent on the intersomatic distance between recorded neurons for a range of 0–160 μm ($P > 0.05$ for each connection type). *B*: reciprocity of synaptic connections was not different from that expected by chance. "Expected" reciprocity was calculated from the product of experimentally determined synaptic connection probabilities for each combination of excitatory and inhibitory GABAergic neurons. "Measured" reciprocity is the fraction of experimentally found reciprocal synaptic connections. *C*: amplitudes of unitary synaptic connections were not different for unidirectionally and reciprocally coupled pairs of neurons. Data are means ± SE. Significance was assessed by unpaired *t*-test.

apses from FS or NFS GABAergic neurons and measured the effect of stimulating various numbers of excitatory neurons. Turning off NFS-mediated inhibition had no effect on the number of postsynaptic spiking excitatory neurons in the network (Fig. 8*G*). However, turning off FS-mediated inhibition approximately doubled the number of spiking postsynaptic excitatory neurons (Fig. 8*G*). In the computational model, the rapid recruitment of FS GABAergic neurons thus contributes to preventing postsynaptic excitatory neurons in the network from firing synaptically driven APs.

We next wondered whether our computational modeling based on in vitro brain slice data might help understand

Table 4. *Reciprocally connected neurons were not observed with probabilities different from chance*

	EXC	FS	NFS
EXC			
No. of pairs tested	57	36	46
No. of measured reciprocal connections	2	12	6
Measured reciprocity, %	3.5	33.3	13.0
Expected reciprocity, %	2.8	34.5	11.4
Confidence interval, %	0.0–7.0	19.4–50.0	2.2–19.6
FS			
No. of pairs tested		10	29
No. of measured reciprocal connections		4	2
Measured reciprocity, %		40.0	6.9
Expected reciprocity, %		30.3	9.2
Confidence interval, %		10.0–60.0	0.0–17.2
NFS			
No. of pairs tested			12
No. of measured reciprocal connections			3
Measured reciprocity, %			25.0
Expected reciprocity, %			14.5
Confidence interval, %			0.0–33.3

The probability of finding reciprocal synaptic connections between pairs of neurons measured experimentally was not different compared with the expected probability of reciprocal connections in a network with randomly assigned connectivity. All values of measured reciprocity were inside the confidence intervals computed for the neuron type pairing. The confidence interval denotes the range of values for which measured reciprocity would not be significantly different from the expected reciprocity ($P > 0.05$) given the limited sample size.

basic aspects of neocortical network activity measured in vivo. The lack of spontaneous activity in our membrane potential recordings in vitro forms the most obvious difference with in vivo data (Haider and McCormick 2009). During anesthesia or quiet behavioral states, membrane potential fluctuations are highly correlated in nearby excitatory, FS GABAergic, and NFS GABAergic neurons (Gentet et al. 2010; Lampl et al. 1999; Petersen et al. 2003; Poulet and Petersen 2008; Okun and Lampl 2008). Nearby excitatory, FS GABAergic, and NFS GABAergic neurons in the neocortex therefore depolarize and hyperpolarize synchronously. In deeply anesthetized animals, spontaneously depolarized active neocortical network states (often termed UP states) alternate at slow frequencies (~1 Hz) with quiescent hyperpolarized neocortical network states (often termed DOWN states) (Cowan and Wilson 1994; Steriade et al. 1993). Although there are likely many differences in the neocortical neuronal networks when UP and DOWN states are compared (including possible differences in neuromodulators, short-term synaptic plasticity, activation/inactivation state of different ion channels, and neuronal input resistance), the most obvious difference is simply the instantaneous membrane potential. In our computational model, we therefore investigated whether depolarizing the neocortical neuronal network might alter the effect of stimulating excitatory neurons on the behavior of the neocortical microcircuit (Fig. 8*H*). UP states were mimicked in the computational model by injecting a cell-specific constant depolarizing current such that excitatory neurons depolarized to -51.1 ± 7.2 mV (mean ± SD), FS GABAergic neurons depolarized to -47.8 ± 5.2 mV, and NFS GABAergic neurons depolarized to -48.4 ± 3.7 mV, in close agreement with in vivo experimental measurements (Mateo et al. 2011). In the computational model, stimulation of excitatory neurons during UP states evoked more APs in all three classes of postsynaptic neurons compared with the same stimuli delivered during DOWN states (Fig. 8*I*). For small stimulus sizes (up to ~50 excitatory neurons), UP states strongly enhanced postsynaptic recruitment of both FS and NFS GABAergic neurons (Fig. 8*I*). As stimulus size increased, the response of FS GABAergic neurons saturated, but UP states continued to strongly enhance synaptically driven AP firing in NFS GABAergic neurons (Fig. 8*I*). Although excitatory neurons were also depolarized during UP states, only very few postsynaptic excitatory neurons were driven to fire APs. For a stimulus of 50 excitatory neurons, only 0.06 ± 0.06% of postsynaptic excitatory neurons were recruited from the UP state (compared with UP state responses in 92 ± 1% of FS GABAergic neurons and 12 ± 3% of NFS GABAergic neurons) (Fig. 8*J*). For a stimulus of 100 excitatory neurons, only 0.3 ± 0.1% of postsynaptic excitatory neurons were recruited from the UP state (compared with UP state responses in 100 ± 0% of FS GABAergic neurons and 40 ± 2% of NFS GABAergic neurons) (Fig. 8*J*). In our highly simplified computational modeling of UP states, we therefore found sparse evoked AP firing in excitatory neurons compared with the strong recruitment of inhibitory GABAergic neurons. GABAergic neurons were recruited in a state-dependent manner, with more AP firing from the UP state. Because of the rapid saturation of responses in FS GABAergic neurons, the recruitment of NFS GABAergic neurons showed a stronger state dependence, in good agreement with experimental in vivo data (Mateo et al. 2011).

DISCUSSION

Our data point to a profound role for PV-expressing GABAergic FS neurons in mediating fast local inhibition within layer 2/3 mouse barrel cortex. Therefore, our results are in good agreement with a large body of previous work showing a key role for FS GABAergic neurons in mediating rapid cortical inhibition in hippocampal circuits (Bartos et al. 2007; Freund and Katona 2007; Klausberger and Somogyi 2008; Pouille et al. 2009), in the L4 processing of thalamocortical input (Chittajallu and Isaac 2010; Cruikshank et al. 2007, 2010; Daw et al. 2007; Gabernet et al. 2005; Gibson et al. 1999; Hull et al. 2009; Sun et al. 2006; Tan et al. 2008), and in local neocortical microcircuits (Cardin et al. 2009; Gentet et al. 2010; Gupta et al. 2000; Holmgren et al. 2003; Mateo et al. 2011; Packer and Yuste 2011; Reyes et al. 1998; Sohal et al. 2009; Xu and Callaway 2009).

Many differing features have been described for neocortical GABAergic neurons, and it is currently unclear how to define the most relevant subtypes (Ascoli et al. 2008; Burkhalter 2008; Klausberger and Somogyi 2008; Markram et al. 2004). In the present study, we used mice expressing GFP in almost the entire population of layer 2/3 GABAergic neurons, subdividing them into FS PV-expressing GABAergic neurons (likely mainly comprising perisomatic-targeting and axo-axonic cells) and NFS PV-negative GABAergic neurons (likely mainly comprising 5-HT_{3A}-

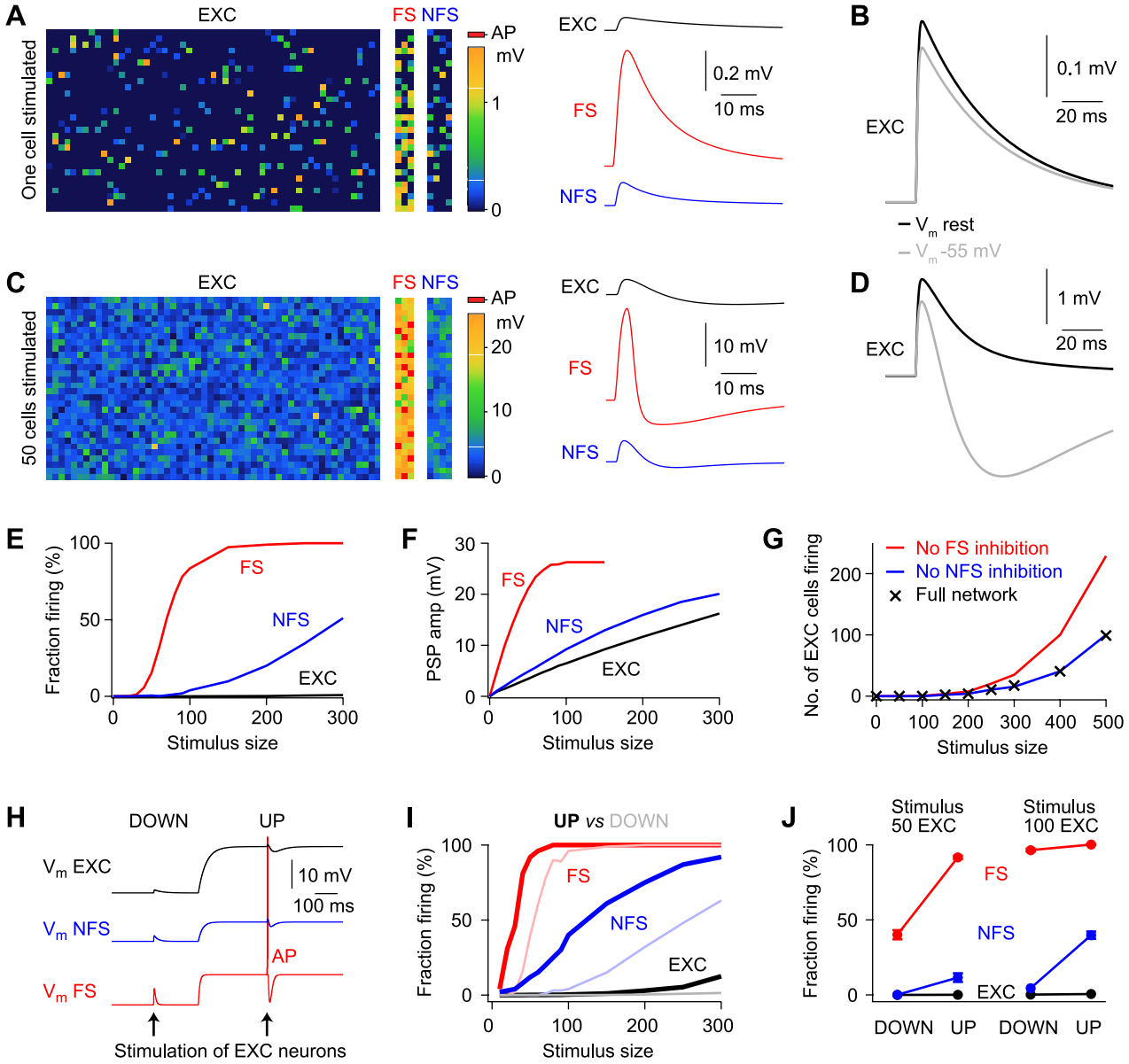

Fig. 8. Computational modeling of the synaptically connected L2/3 neuronal network. *A*: a single AP was evoked in a randomly chosen EXC neuron of the simulated L2/3 network. Each pixel in the matrices (*left*) represents a single neuron, color coded according to the excitatory PSP (EPSP) peak amplitude. AP firing in a single presynaptic EXC neuron evoked sparse EPSPs in other EXC neurons and in NFS GABAergic neurons, whereas a large fraction of FS GABAergic neurons depolarized. The grand average time courses (*right*) show EPSPs evoked by a single presynaptic EXC neuron averaged across all neurons. *B*: EPSP in a randomly chosen EXC neuron evoked by stimulation of a single EXC neuron measured at resting V_m (black trace) and when depolarized to −55 mV (gray trace). *C*: color-coded matrices (*left*) and grand average time courses (*right*) of PSPs in the network evoked by synchronous stimulation of 50 EXC neurons, each firing a single AP. *D*: PSP of a randomly chosen EXC neuron in response to stimulation of 50 EXC neurons measured at resting V_m (black trace) and when depolarized to −55 mV (gray trace). *E*: fraction of postsynaptically spiking neurons vs. the number of presynaptically spiking neurons in the simulated network. *F*: average cell type-specific PSP amplitudes vs. stimulus size. *G*: number of postsynaptic EXC neurons firing APs vs. stimulus size for the full network (black crosses), without NFS inhibition (blue trace), and without FS inhibition (red trace). *H*: highly simplified model of UP states through depolarization of EXC, FS GABAergic, and NFS GABAergic neurons. In this example, stimulation of EXC neurons during the UP state evoked a synaptically driven AP in the FS GABAergic neuron. *I*: fraction of postsynaptic neurons (color coded according to cell type) firing synaptically driven APs as a function of the number of EXC neurons stimulated during DOWN (thin curves) and UP states (thick curves). *J*: fraction of postsynaptic neurons firing APs evoked by a stimulus size of 50 (*left*) and 100 EXC neurons (*right*) in DOWN and UP states.

expressing and nicotinic ACh receptor-expressing cells) (Lee et al. 2010). Future investigations of genetically engineered mice expressing GFP or cre recombinase in specific subtypes of GABAergic neurons will be of great interest (Taniguchi et al. 2011).

Our experiments were conducted in GAD67-GFP knockin mice (Tamamaki et al. 2003), which may have altered inhibition in visual cortex (Chattopadhyaya et al. 2007; Runyan et al. 2010; but see also Kerlin et al. 2010, where no differences were found compared with wild-type mice). However, previous investigations in barrel cortex of GAD67-GFP mice compared with wild-type mice did not reveal differences in evoked inhibitory postsynaptic currents (IPSCs) in vitro (Gentet et al. 2010), in miniature IPSCs in vitro (Gentet et al. 2010), or in firing rates of excitatory

layer 2/3 neurons in awake mice (Crochet and Petersen 2006; Crochet et al. 2011; Gentet et al. 2010; Poulet and Petersen 2008).

FS PV-expressing GABAergic neurons receive strong excitatory synaptic input from nearby excitatory neurons in layer 2/3 mouse barrel cortex. In response to optogenetic stimulation of excitatory neurons, GABAergic FS neurons received larger and faster depolarizing PSPs compared with excitatory neurons and GABAergic NFS neurons in layer 2/3 mouse barrel cortex. These optogenetic data obtained in vitro (where we found a cell type-specific PSP amplitude ratio of EXC/NFS/FS = 1:1.8:4.8) are in close agreement with results from similar optogenetic experiments carried out in vivo in layer 2/3 mouse barrel cortex (PSP amplitude ratio of EXC/NFS/FS = 1:1.9:5.4) (Mateo et al. 2011). Furthermore, the optogenetic stimulation of excitatory neurons in vitro drove APs predominantly in GABAergic FS neurons with little firing in postsynaptic excitatory and GABAergic NFS neurons, which also agrees well with data from similar in vivo experiments in which FS neurons are more strongly recruited by the optogenetic stimulus compared with NFS GABAergic and excitatory neurons (Mateo et al. 2011).

To obtain a mechanistic understanding of these optogenetically evoked network responses, we probed the underlying synaptic connectivity of the layer 2/3 neocortical microcircuit in vitro through simultaneous whole cell recordings. GABAergic FS neurons received unitary glutamatergic synaptic inputs with higher probability, shorter latency, more rapid rise time, and larger amplitude compared with excitatory neurons and GABAergic NFS neurons. These data agree with previous studies of neocortical layer 2/3 microcircuits in which the excitatory synaptic output connectivity onto other excitatory neurons has been investigated compared with that onto FS PV-expressing GABAergic neurons (Hofer et al. 2011; Holmgren et al. 2003).

Given the very high rate of synaptic connectivity from excitatory to GABAergic FS neurons (58%), it is difficult to envision receptive fields in GABAergic FS neurons with as high a specificity as found for excitatory neurons. In agreement with such a microcircuit-based hypothesis, in vivo recordings of GABAergic FS neurons in general have found broader receptive fields for GABAergic FS neurons compared with excitatory neurons in neocortex (Hofer et al. 2011; Kerlin et al. 2010; Liu et al. 2009; Swadlow and Gusev 2002; but see also Runyan et al. 2010).

As experimental data gradually becomes more quantitative, it will become increasingly important to apply computational modeling to understand neuronal network dynamics. Our highly simplified neuronal network model (based on somatic measurements of synaptic potentials and intrinsic electrophysiological properties) did not incorporate dendrites, gap junctions, or voltage-gated conductances but nonetheless was able to account for several important features observed experimentally in vitro. Stimulation of excitatory layer 2/3 neurons in the model evoked synaptically driven APs predominantly in FS GABAergic neurons, similar to the experimental optogenetic observations. The ratios of PSPs observed in excitatory neurons and NFS GABAergic neurons relative to FS GABAergic neurons were also similar in the computational model (EXC/NFS/FS = 1:1.4:6.3) and the in vitro experimental optogenetic data (EXC/NFS/FS = 1:1.8:4.8). However, it should be noted that GABAergic FS neurons in the model received relatively larger PSPs than were experimentally measured. In part, this likely reflects our inability to quantify PSP amplitude when the postsynaptic neuron is spiking, and therefore our optogenetic experimental measure of excitatory input onto FS GABAergic neurons will be underestimated. In addition, there may well be interesting cell type-specific differences in dendritic synaptic integration (Stuart et al. 2008). Furthermore, there could be effects on connectivity based on the relative locations of somata with respect to barrel column and septal columns (Alloway 2008; Brecht et al. 2003; Lübke and Feldmeyer 2007), which were not analyzed in the current study.

Disynaptic inhibition driven by FS GABAergic neurons. Because GABAergic FS neurons were the main class of neurons that were recruited by the optogenetic stimulus to fire APs, the disynaptic inhibition recorded in postsynaptic excitatory neurons was likely to be mediated largely by GABAergic FS neurons under our experimental conditions. Analysis of unitary synaptic connectivity established that GABAergic FS neurons provided a strong and rapid inhibitory output onto surrounding layer 2/3 neurons with particularly high probabilities of synaptic connections onto excitatory and other GABAergic FS neurons. These data are in good agreement with a recent study showing dense inhibitory connectivity of PV-expressing neurons innervating excitatory layer 2/3 neurons (Packer and Yuste 2011). In the computational model, this disynaptic FS GABAergic inhibition was sufficiently strong and rapid to reduce evoked spiking activity in postsynaptic excitatory neurons. It will be of great interest in future experiments to directly test this prediction through inactivation of FS GABAergic neurons, which perhaps could be accomplished by conditionally expressing halorhodopsin in PV-cre mice (Cardin et al. 2009; Sohal et al. 2009; Zhang et al. 2007).

GABAergic NFS neurons also densely innervated nearby excitatory, FS GABAergic, and other NFS GABAergic neurons in layer 2/3 barrel cortex. Although FS GABAergic neurons appeared to provide the most important source of inhibition when small numbers of excitatory neurons were stimulated, GABAergic NFS neurons were increasingly recruited at larger stimulus strengths. GABAergic NFS neurons therefore expand the dynamic range of inhibition and could be viewed as providing a secondary backup inhibition, which might be especially useful under conditions when the GABAergic FS neurons are operating at near saturation. Similarly, during depolarized network states in vivo, the recruitment of GABAergic NFS neurons by optogenetic stimulation plays a relatively more important role compared with that during hyperpolarized network states (Mateo et al. 2011), a result also predicted by our computational modeling (Fig. 8, *I* and *J*).

In this study, we exclusively investigated the effect of a single near-synchronous stimulation of excitatory neurons. Neocortical GABAergic neurons in vitro receive excitatory input strongly modulated by short-term synaptic plasticity. Whereas PV-expressing GABAergic FS neurons receive strongly depressing excitatory synaptic input, somatostatin-expressing GABAergic neurons (which include Martinotti cells) receive strongly facilitating excitatory synaptic input (Fanselow et al. 2008; Kapfer et al. 2007; Reyes et al. 1998; Silberberg and Markram 2007). Consistent with such strongly facilitating synaptic inputs, previous studies have implicated somatostatin-expressing GABAergic neurons in mediating disynaptic inhibition driven by high-frequency firing in excitatory cortical neurons in the neocortex (Kapfer et al. 2007; Silberberg and

Markram 2007). Interestingly, these somatostatin-expressing GABAergic neurons have recently been shown to densely innervate nearby layer 2/3 excitatory neurons (Fino and Yuste 2011). The dense inhibitory innervation of excitatory neurons we observed for FS and NFS GABAergic neurons might thus be a common motif among the different types of inhibitory neocortical GABAergic neurons (Packer and Yuste 2011).

Although our data point to a critical role for FS GABAergic neurons in mediating disynaptic inhibition under our experimental conditions in vitro (this study) and in vivo (Mateo et al. 2011), it is important to note that the relative importance of different classes of GABAergic neurons in controlling cortical dynamics will likely depend on many factors, including the number and pattern of active neurons, cortical state, neuromodulators, and recent history of cortical activity.

Sparse AP firing in excitatory layer 2/3 neurons in vivo might result from strong and rapid inhibition driven primarily by FS GABAergic neurons. In vivo recordings indicate sparse AP firing in excitatory layer 2/3 barrel cortex neurons, even during active whisker behaviors (Crochet and Petersen 2006; Crochet et al. 2011; de Kock and Sakmann 2009; Gentet et al. 2010; O'Connor et al. 2010; Poulet and Petersen 2008). However, in vivo AP firing rates for GABAergic neurons are substantially higher, especially for GABAergic FS neurons that overall fire at the highest rates in layer 2/3 mouse barrel cortex (Gentet et al. 2010; Mateo et al. 2011). Our current in vitro synaptic circuit analysis of layer 2/3 provides mechanistic insight into these cell type-specific in vivo firing rates. The strong excitatory synaptic connections from layer 2/3 pyramidal neurons onto GABAergic FS neurons, which we found were able to drive substantial postsynaptic firing in vitro, are also likely to contribute to driving the high firing rates of GABAergic FS neurons in vivo. Conversely, the high rates of inhibitory synaptic connectivity from GABAergic neurons onto excitatory layer 2/3 neurons found in vitro might help enforce sparse AP coding in excitatory layer 2/3 neurons in vivo (Crochet and Petersen 2006; Crochet et al. 2011; Gentet et al. 2010; Mateo et al. 2011; O'Connor et al. 2010; Poulet and Petersen 2008; Sakata and Harris 2009). Specifically, the rapid recruitment of GABAergic FS neurons likely provides part of the fast inhibition driving the hyperpolarized reversal potentials of active touch responses recorded in excitatory layer 2/3 barrel cortex neurons (Crochet et al. 2011). Similarly, the rapid recruitment of FS GABAergic neurons by optogenetic stimulation of excitatory neurons in vivo is likely involved in driving nearby excitatory neurons towards reversal potentials that are hyperpolarized relative to action potential threshold (Mateo et al. 2011). Thereby, the optogenetic stimulation of excitatory layer 2/3 neurons in vivo in fact evokes a counterintuitive decrease in AP firing in surrounding excitatory neurons (Mateo et al. 2011). Taken together, our in vitro data (this study) and our related in vivo data (Mateo et al. 2011) suggest that disynaptic inhibition driven by FS GABAergic neurons in the neocortex mediates competition among excitatory neurons such that perhaps only a small fraction of excitatory layer 2/3 neurons can be active at any given time.

ACKNOWLEDGMENTS

We thank Karl Deisseroth for ChR2-mCherry plasmid and Rachel Aronoff for help with lentivector production.

GRANTS

This work was funded by grants from the Swiss National Science Foundation, Human Frontier Science Program, SystemsX.ch, National Centers of Competence in Research Synapsy and European Union Framework 7 Information and Communication Technologies Project 215910 (BIOTACT).

DISCLOSURES

No conflicts of interest, financial or otherwise, are declared by the authors.

AUTHOR CONTRIBUTIONS

Author contributions: M.A., C.T., C.M., W.G., and C.C.P. conception and design of research; M.A. and C.T. performed experiments; M.A. and C.T. analyzed data; M.A., C.T., C.M., W.G., and C.C.P. interpreted results of experiments; M.A., C.T., and C.C.P. prepared figures; M.A., C.T., and C.C.P. drafted manuscript; M.A., C.T., C.M., W.G., and C.C.P. edited and revised manuscript; M.A., C.T., C.M., W.G., and C.C.P. approved final version of manuscript.

REFERENCES

Alloway KD. Information processing streams in rodent barrel cortex: the differential functions of barrel and septal circuits. *Cereb Cortex* 18: 979–989, 2008.

Aronoff R, Petersen CC. Layer, column and cell-type specific genetic manipulation in mouse barrel cortex. *Front Neurosci* 2: 64–71, 2008.

Ascoli GA, Alonso-Nanclares L, Anderson SA, Barrionuevo G, Benavides-Piccione R, Burkhalter A, Buzsáki G, Cauli B, DeFelipe J, Fairén A, Feldmeyer D, Fishell G, Fregnac Y, Freund TF, Gardner D, Gardner EP, Goldberg JH, Helmstaedter M, Hestrin S, Karube F, Kisvárday ZF, Lambolez B, Lewis DA, Marin O, Markram H, Muñoz A, Packer A, Petersen CCH, Rockland KS, Rossier J, Rudy B, Somogyi P, Staiger JF, Tamas G, Thomson AM, Toledo-Rodriguez M, Wang Y, West DC, Yuste R. Petilla terminology: nomenclature of features of GABAergic interneurons of the cerebral cortex. *Nat Rev Neurosci* 9: 557–568, 2008.

Bartos M, Vida I, Jonas P. Synaptic mechanisms of synchronized gamma oscillations in inhibitory interneuron networks. *Nat Rev Neurosci* 8: 45–56, 2007.

Bock DD, Lee WC, Kerlin AM, Andermann ML, Hood G, Wetzel AW, Yurgenson S, Soucy ER, Kim HS, Reid RC. Network anatomy and in vivo physiology of visual cortical neurons. *Nature* 471: 177–182, 2011.

Boyden ES, Zhang F, Bamberg E, Nagel G, Deisseroth K. Millisecond-timescale, genetically targeted optical control of neural activity. *Nat Neurosci* 8: 1263–1268, 2005.

Brecht M, Roth A, Sakmann B. Dynamic receptive fields of reconstructed pyramidal cells in layers 3 and 2 of rat somatosensory barrel cortex. *J Physiol* 553: 243–265, 2003.

Brette R, Gerstner W. Adaptive exponential integrate-and-fire model as an effective description of neuronal activity. *J Neurophysiol* 94: 3637–3642, 2005.

Brown SP, Hestrin S. Intracortical circuits of pyramidal neurons reflect their long-range axonal targets. *Nature* 457: 1133–1136, 2009.

Bureau I, von Saint Paul F, Svoboda K. Interdigitated paralemniscal and lemniscal pathways in the mouse barrel cortex. *PLoS Biol* 4: e382, 2006.

Burkhalter A. Many specialists for suppressing cortical excitation. *Front Neurosci* 2: 155–167, 2008.

Cardin JA, Carlén M, Meletis K, Knoblich U, Zhang F, Deisseroth K, Tsai LH, Moore CI. Driving fast-spiking cells induces gamma rhythm and controls sensory responses. *Nature* 459: 663–667, 2009.

Cauli B, Audinat E, Lambolez B, Angulo MC, Ropert N, Tsuzuki K, Hestrin S, Rossier J. Molecular and physiological diversity of cortical nonpyramidal cells. *J Neurosci* 17: 3894–3906, 1997.

Chattopadhyaya B, Di Cristo G, Wu CZ, Knott G, Kuhlman S, Fu Y, Palmiter RD, Huang ZJ. GAD67-mediated GABA synthesis and signaling regulate inhibitory synaptic innervation in the visual cortex. *Neuron* 54: 889–903, 2007.

Chittajallu R, Isaac JT. Emergence of cortical inhibition by coordinated sensory-driven plasticity at distinct synaptic loci. *Nat Neurosci* 13: 1240–1248, 2010.

Clopath C, Büsing L, Vasilaki E, Gerstner W. Connectivity reflects coding: a model of voltage-based STDP with homeostasis. *Nat Neurosci* 13: 344–352, 2010.

Cowan RL, Wilson CJ. Spontaneous firing patterns and axonal projections of single corticostriatal neurons in the rat medial agranular cortex. *J Neurophysiol* 71:17–32, 1994.

Crochet S, Petersen CC. Correlating whisker behavior with membrane potential in barrel cortex of awake mice. *Nat Neurosci* 9: 608–610, 2006.

Crochet S, Poulet JF, Kremer Y, Petersen CC. Synaptic mechanisms underlying sparse coding of active touch. *Neuron* 69: 1160–1175, 2011.

Cruikshank SJ, Lewis TJ, Connors BW. Synaptic basis for intense thalamocortical activation of feedforward inhibitory cells in neocortex. *Nat Neurosci* 10: 462–468, 2007.

Cruikshank SJ, Urabe H, Nurmikko AV, Connors BW. Pathway-specific feedforward circuits between thalamus and neocortex revealed by selective optical stimulation of axons. *Neuron* 65: 230–245, 2010.

Davison AP, Bruderle D, Eppler JM, Kremkow J, Muller E, Pecevski D, Perrinet L, Yger P. PyNN: a common interface for neuronal network simulators. *Front Neuroinform* 2: 11, 2008.

Daw MI, Ashby MC, Isaac JT. Coordinated developmental recruitment of latent fast spiking interneurons in layer IV barrel cortex. *Nat Neurosci* 10: 453–461, 2007.

Deglon N, Tseng JL, Bensadoun JC, Zurn AD, Arsenijevic Y, Pereira de Almeida L, Zufferey R, Trono D, Aebischer P. Self-inactivating lentiviral vectors with enhanced transgene expression as potential gene transfer system in Parkinson's disease. *Hum Gene Ther* 11: 179–190, 2000.

de Kock CP, Sakmann B. Spiking in primary somatosensory cortex during natural whisking in awake head-restrained rats is cell-type specific. *Proc Natl Acad Sci USA* 106: 16446–16450, 2009.

Fanselow EE, Richardson KA, Connors BW. Selective, state-dependent activation of somatostatin-expressing inhibitory interneurons in mouse neocortex. *J Neurophysiol* 100: 2640–2652, 2008.

Feldmeyer D, Lübke J, Sakmann B. Efficacy and connectivity of intracolumnar pairs of layer 2/3 pyramidal cells in the barrel cortex of juvenile rats. *J Physiol* 575: 583–602, 2006.

Fino E, Yuste R. Dense inhibitory connectivity in neocortex. *Neuron* 69: 1188–1203, 2011.

Freund TF, Katona I. Perisomatic inhibition. *Neuron* 56: 33–42, 2007.

Gabernet L, Jadhav SP, Feldman DE, Carandini M, Scanziani M. Somatosensory integration controlled by dynamic thalamocortical feed-forward inhibition. *Neuron* 48: 315–327, 2005.

Galarreta M, Hestrin S. A network of fast-spiking cells in the neocortex connected by electrical synapses. *Nature* 402: 72–75, 1999.

Gentet LJ, Avermann M, Matyas F, Staiger JF, Petersen CC. Membrane potential dynamics of GABAergic neurons in the barrel cortex of behaving mice. *Neuron* 65: 422–435, 2010.

Gerstner W, Kistler W. *Spiking Neuron Models: Single Neurons, Populations, Plasticity.* Cambridge: Cambridge University Press, 2002.

Gewaltig MO, Diesmann M. NEST (neural simulation tool). *Scholarpedia* 2: 1430, 2007.

Gibson JR, Beierlein M, Connors BW. Two networks of electrically coupled inhibitory neurons in neocortex. *Nature* 402: 75–79, 1999.

Gupta A, Wang Y, Markram H. Organizing principles for a diversity of GABAergic interneurons and synapses in the neocortex. *Science* 287: 273–278, 2000.

Haider B, McCormick DA. Rapid neocortical dynamics: cellular and network mechanisms. *Neuron* 62: 171–189, 2009.

Helmstaedter M, Staiger JF, Sakmann B, Feldmeyer D. Efficient recruitment of layer 2/3 interneurons by layer 4 input in single columns of rat somatosensory cortex. *J Neurosci* 28: 8273–8284, 2008.

Hofer SB, Ko H, Pichler B, Vogelstein J, Ros H, Zeng H, Lein E, Lesica NA, Mrsic-Flogel TD. Differential connectivity and response dynamics of excitatory and inhibitory neurons in visual cortex. *Nat Neurosci* 14: 1045–1052, 2011.

Holmgren C, Harkany T, Svennenfors B, Zilberter Y. Pyramidal cell communication within local networks in layer 2/3 of rat neocortex. *J Physiol* 551: 139–153, 2003.

Hull C, Isaacson JS, Scanziani M. Postsynaptic mechanisms govern the differential excitation of cortical neurons by thalamic inputs. *J Neurosci* 29: 9127–9136, 2009.

Kampa BM, Letzkus JJ, Stuart GJ. Cortical feed-forward networks for binding different streams of sensory information. *Nat Neurosci* 9: 1472–1473, 2006.

Kapfer C, Glickfeld LL, Atallah BV, Scanziani M. Supralinear increase of recurrent inhibition during sparse activity in the somatosensory cortex. *Nat Neurosci* 10: 743–753, 2007.

Kawaguchi Y, Kubota Y. Correlation of physiological subgroupings of nonpyramidal cells with parvalbumin- and calbindinD28k-immunoreactive neurons in layer V of rat frontal cortex. *J Neurophysiol* 70: 387–396, 1993.

Kawaguchi Y. Physiological subgroups of nonpyramidal cells with specific morphological characteristics in layer II/III of rat frontal cortex. *J Neurosci* 15: 2638–2655, 1995.

Kerlin AM, Andermann ML, Berezovskii VK, Reid RC. Broadly tuned response properties of diverse inhibitory neuron subtypes in mouse visual cortex. *Neuron* 67: 858–871, 2010.

Klausberger T, Somogyi P. Neuronal diversity and temporal dynamics: the unity of hippocampal circuit operations. *Science* 321: 53–57, 2008.

Ko H, Hofer SB, Pichler B, Buchanan KA, Sjostrom PJ, Mrsic-Flogel TD. Functional specificity of local synaptic connections in neocortical networks. *Nature* 473: 87–91, 2011.

Lampl I, Reichova I, Ferster D. Synchronous membrane potential fluctuations in neurons of the cat visual cortex. *Neuron* 22: 361–374, 1999.

Lee S, Hjerling-Leffler J, Zagha E, Fishell G, Rudy B. The largest group of superficial neocortical GABAergic interneurons expresses ionotropic serotonin receptors. *J Neurosci* 30, 16796–16808, 2010.

Lefort S, Tomm C, Sarria JC, Petersen CC. The excitatory neuronal network of the C2 barrel column in mouse primary somatosensory cortex. *Neuron* 61: 301–316, 2009.

Liu BH, Li P, Li YT, Sun YJ, Yanagawa Y, Obata K, Zhang LI, Tao HW. Visual receptive field structure of cortical inhibitory neurons revealed by two-photon imaging guided recording. *J Neurosci* 29: 10520–10532, 2009.

Lübke J, Roth A, Feldmeyer D, Sakmann B. Morphometric analysis of the columnar innervation domain of neurons connecting layer 4 and layer 2/3 of juvenile rat barrel cortex. *Cereb Cortex* 13: 1051–1063, 2003.

Lübke J, Feldmeyer D. Excitatory signal flow and connectivity in a cortical column: focus on barrel cortex. *Brain Struct Funct* 212: 3–17, 2007.

Markram H, Lübke J, Frotscher M, Roth A, Sakmann B. Physiology and anatomy of synaptic connections between thick tufted pyramidal neurones in the developing rat neocortex. *J Physiol* 500: 409–440, 1997.

Markram H, Toledo-Rodriguez M, Wang Y, Gupta A, Silberberg G, Wu C. Interneurons of the neocortical inhibitory system. *Nat Rev Neurosci* 5: 793–807, 2004.

Mateo C, Avermann M, Gentet LJ, Zhang F, Deisseroth K, Petersen CC. In vivo optogenetic stimulation of neocortical excitatory neurons drives brain-state-dependent inhibition. *Curr Biol* 21: 1593–1602, 2011.

Molnár G, Oláh S, Komlósi G, Füle M, Szabadics J, Varga C, Barzó P, Tamás G. Complex events initiated by individual spikes in the human cerebral cortex. *PLoS Biol* 6: e222, 2008.

Nagel G, Szellas T, Huhn W, Kateriya S, Adeishvili N, Berthold P, Ollig D, Hegemann P, Bamberg E. Channelrhodopsin-2, a directly light-gated cation-selective membrane channel. *Proc Natl Acad Sci USA* 100: 13940–13945, 2003.

Nathanson JL, Yanagawa Y, Obata K, Callaway EM. Preferential labeling of inhibitory and excitatory cortical neurons by endogenous tropism of adeno-associated virus and lentivirus vectors. *Neuroscience* 161: 441–450, 2009.

O'Connor DH, Peron SP, Huber D, Svoboda K. Neural activity in barrel cortex underlying vibrissa-based object localization in mice. *Neuron* 67: 1048–1061, 2010.

Okun M, Lampl I. Instantaneous correlation of excitation and inhibition during ongoing and sensory-evoked activities. *Nat Neurosci* 11: 535–537, 2008.

Oláh S, Füle M, Komlósi G, Varga C, Báldi R, Barzó P, Tamás G. Regulation of cortical microcircuits by unitary GABA-mediated volume transmission. *Nature* 461: 1278–1281, 2009.

Packer AM, Yuste R. Dense, unspecific connectivity of neocortical parvalbumin-positive interneurons: a canonical microcircuit for inhibition? *J Neurosci* 31: 13260–13271, 2011.

Perin R, Berger TK, Markram H. A synaptic organizing principle for cortical neuronal groups. *Proc Natl Acad Sci USA* 108: 5419–5424, 2011.

Petersen CC, Hahn TT, Mehta M, Grinvald A, Sakmann B. Interaction of sensory responses with spontaneous depolarization in layer 2/3 barrel cortex. *Proc Natl Acad Sci USA* 100: 13638–13643, 2003.

Petersen CC. The functional organization of the barrel cortex. *Neuron* 56: 339–355, 2007.

Pouille F, Marin-Burgin A, Adesnik H, Atallah BV, Scanziani M. Input normalization by global feedforward inhibition expands cortical dynamic range. *Nat Neurosci* 12: 1577–1585, 2009.

Poulet JF, Petersen CC. Internal brain state regulates membrane potential synchrony in barrel cortex of behaving mice. *Nature* 454: 881–885, 2008.

Reyes AD, Lujan R, Rozov A, Burnashev N, Somogyi P, Sakmann B. Target-cell-specific facilitation and depression in neocortical circuits. *Nat Neurosci* 1: 279–285, 1998.

Runyan CA, Schummers J, Van Wart A, Kuhlman SJ, Wilson NR, Huang ZJ, Sur M. Response features of parvalbumin-expressing interneurons suggest precise roles for subtypes of inhibition in visual cortex. *Neuron* 67: 847–857, 2010.

Sakata S, Harris KD. Laminar structure of spontaneous and sensory-evoked population activity in auditory cortex. *Neuron* 64: 404–418, 2009.

Schubert D, Kötter R, Staiger JF. Mapping functional connectivity in barrel-related columns reveals layer- and cell type-specific microcircuits. *Brain Struct Funct* 212: 107–119, 2007.

Silberberg G, Markram H. Disynaptic inhibition between neocortical pyramidal cells mediated by Martinotti cells. *Neuron* 53: 735–746, 2007.

Sohal VS, Zhang F, Yizhar O, Deisseroth K. Parvalbumin neurons and gamma rhythms enhance cortical circuit performance. *Nature* 459: 698–702, 2009.

Somogyi P. A specific 'axo-axonal' interneuron in the visual cortex of the rat. *Brain Res* 136: 345–350, 1977.

Song S, Sjöström PJ, Reigl M, Nelson S, Chklovskii DB. Highly nonrandom features of synaptic connectivity in local cortical circuits. *PLoS Biol* 3: e68, 2005.

Steriade M, Nuñez A, Amzica F. A novel slow (<1 Hz) oscillation of neocortical neurons in vivo: depolarizing and hyperpolarizing components. *J Neurosci* 13: 3252–3265, 1993.

Stuart GJ, Spruston N, Häusser M. Dendrites (2nd ed.). Oxford: Oxford University Press, 2008.

Sun QQ, Huguenard JR, Prince DA. Barrel cortex microcircuits: thalamocortical feedforward inhibition in spiny stellate cells is mediated by a small number of fast-spiking interneurons. *J Neurosci* 26: 1219–1230, 2006.

Swadlow HA, Gusev AG. Receptive-field construction in cortical inhibitory interneurons. *Nat Neurosci* 5: 403–404, 2002.

Tan Z, Hu H, Huang ZJ, Agmon A. Robust but delayed thalamocortical activation of dendritic-targeting inhibitory interneurons. *Proc Natl Acad Sci USA* 105: 2187–2192, 2008.

Taniguchi H, He M, Wu P, Kim S, Paik R, Sugino K, Kvitsani D, Fu Y, Lu J, Lin Y, Miyoshi G, Shima Y, Fishell G, Nelson SB, Huang ZJ. A resource of Cre driver lines for genetic targeting of GABAergic neurons in cerebral cortex. *Neuron* 71: 995–1013, 2011.

Tamamaki N, Yanagawa Y, Tomioka R, Miyazaki J, Obata K, Kaneko T. Green fluorescent protein expression and colocalization with calretinin, parvalbumin, and somatostatin in the GAD67-GFP knock-in mouse. *J Comp Neurol* 467: 60–79, 2003.

Thomson AM, Lamy C. Functional maps of neocortical local circuitry. *Front Neurosci* 1:19–42, 2007.

Xu X, Callaway EM. Laminar specificity of functional input to distinct types of inhibitory cortical neurons. *J Neurosci* 29: 70–85, 2009.

Yoshimura Y, Dantzker JL, Callaway EM. Excitatory cortical neurons form fine-scale functional networks. *Nature* 433: 868–873, 2005.

Zhang F, Wang LP, Brauner M, Liewald JF, Kay K, Watzke N, Wood PG, Bamberg E, Nagel G, Gottschalk A, Deisseroth K. Multimodal fast optical interrogation of neural circuitry. *Nature* 446: 633–639, 2007.